

UC Davis

UC Davis Previously Published Works

Title

Astrocytes follow ganglion cell axons to establish an angiogenic template during retinal development

Permalink

<https://escholarship.org/uc/item/26h510gv>

Journal

Glia, 65(10)

ISSN

0894-1491

Authors

O'Sullivan, Matthew L
Puñal, Vanessa M
Kerstein, Patrick C
[et al.](#)

Publication Date

2017-10-01


DOI

10.1002/glia.23189

Peer reviewed

RESEARCH ARTICLE

Astrocytes follow ganglion cell axons to establish an angiogenic template during retinal development

Matthew L. O'Sullivan^{1,2} | Vanessa M. Puñal^{1,2} | Patrick C. Kerstein³ |
Joseph A. Brzezinski IV⁴ | Tom Glaser⁵ | Kevin M. Wright³ | Jeremy N. Kay^{1,2} 

¹Department of Neurobiology, Duke University School of Medicine, Durham, North Carolina 27710

²Department of Ophthalmology, Duke University School of Medicine, Durham, North Carolina 27710

³Vollum Institute, Oregon Health and Science University, Portland, Oregon 97239

⁴Department of Ophthalmology, University of Colorado Denver, Aurora, Colorado 80045

⁵Department of Cell Biology & Human Anatomy, University of California, Davis, California 95616

Correspondence

Jeremy Kay, Duke Eye Center, Box 3802, Durham, NC 27710, USA.
Email: jeremy.kay@duke.edu

Funding information

National Eye Institute, Grant/Award Number: R01EY024694; National Eye Institute, Grant/Award Number: EY5722; Ruth K. Broad Foundation; National Science Foundation, Grant/Award Number: DGE-1644868; Pew Charitable Trusts; E. Matilda Ziegler Foundation; McKnight Endowment Fund for Neuroscience; Alfred P. Sloan Foundation; Holland-Trice Scholars Award; Research to Prevent Blindness

Abstract

Immature astrocytes and blood vessels enter the developing mammalian retina at the optic nerve head and migrate peripherally to colonize the entire retinal nerve fiber layer (RNFL). Retinal vascularization is arrested in retinopathy of prematurity (ROP), a major cause of bilateral blindness in children. Despite their importance in normal development and ROP, the factors that control vascularization of the retina remain poorly understood. Because astrocytes form a reticular network that appears to provide a substrate for migrating endothelial cells, they have long been proposed to guide angiogenesis. However, whether astrocytes do in fact impose a spatial pattern on developing vessels remains unclear, and how astrocytes themselves are guided is unknown. Here we explore the cellular mechanisms that ensure complete retinal coverage by astrocytes and blood vessels in mouse. We find that migrating astrocytes associate closely with the axons of retinal ganglion cells (RGCs), their neighbors in the RNFL. Analysis of *Robo1*; *Robo2* mutants, in which RGC axon guidance is disrupted, and *Math5* (*Atoh7*) mutants, which lack RGCs, reveals that RGCs provide directional information to migrating astrocytes that sets them on a centrifugal trajectory. Without this guidance, astrocytes exhibit polarization defects, fail to colonize the peripheral retina, and display abnormal fine-scale spatial patterning. Furthermore, using cell type-specific chemical-genetic tools to selectively ablate astrocytes, we show that the astrocyte template is required for angiogenesis and vessel patterning. Our results are consistent with a model whereby RGC axons guide formation of an astrocytic network that subsequently directs vessel development.

KEYWORDS

angiogenesis, astrocyte, migration, mouse, retinal ganglion cell

1 | INTRODUCTION

In the developing retina, most cell types are born locally, migrating only a short distance to reach their final location. By contrast, astrocytes and blood vessels enter the retina through the optic nerve head during development and must migrate centrifugally to cover the entire face of the retina (Stone & Dreher, 1987; Watanabe & Raff, 1988). How astrocytes and blood vessels colonize the retina remains poorly understood, but this process is of critical importance for the development of a healthy visual system. Indeed, this process is disrupted in retinopathy of prematurity (ROP), a leading cause of devastating bilateral blindness in children (Hellstrom, Smith, & Dammann, 2013). Furthermore,

astrocyte–vascular interactions may contribute to patterning of brain vessels (Ma, Kwon, & Huang, 2012), so insights into development of these cell types in the retina could have broad significance.

Astrocyte–vascular colonization of the retina occurs mostly postnatally in the mouse, and in the second and third trimesters of gestation in humans (Chan-Ling et al., 2004; Chu, Hughes, & Chan-Ling, 2001; Huxlin, Sefton, & Furby, 1992). The sequence of events leading to colonization are described in the literature (Tao & Zhang, 2014) and illustrated in Figure 1. Astrocytes begin migrating first, spreading peripherally from the optic nerve head along the innermost surface of the retina to form a planar, reticular network with honeycomb morphology in the retinal nerve fiber layer (RNFL; Figure 1A,C).

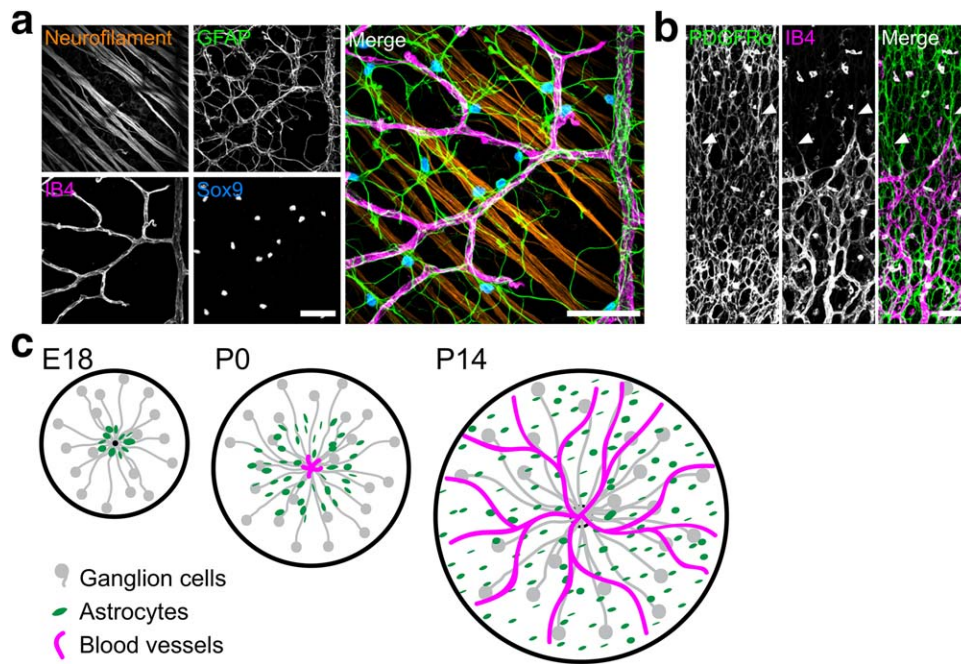


FIGURE 1 Cellular composition and development of the nerve fiber layer. A, Flat-mounted P14 retina imaged at the RNFL level shows its cellular anatomy at a relatively mature stage. Note close spatial proximity of RGC axons (neurofilament), astrocytes (Sox9 and GFAP), and blood vessels (IB4). B, RNFL development: P4 retinal flat-mount stained with anti-PDGFR α (astrocytes, left) and IB4 (vasculature, center) to show the astrocyte reticular network and advancing vascular wavefront. Central retina is at the bottom of the panel; peripheral retina is toward the top. The astrocyte network develops ahead of vasculature and has already colonized peripheral regions at this age. Endothelial tip cells extend filopodia toward the periphery along astrocytes (arrowheads). C, Schematic illustrating the sequential colonization of the RNFL first by RGC axons (gray), then astrocytes (green), and finally blood vessels (magenta). RGC axons exit the retina at the optic nerve head (left panel, black dot); astrocytes and vessels enter at the same point and migrate centrifugally. Scale bar: 50 μ m [Color figure can be viewed at wileyonlinelibrary.com]

Subsequently, developing vessels enter the retina and angiogenesis proceeds in a similar center-to-peripheral pattern (Figure 1A,C). The filopodia of endothelial tip cells at the vascular wavefront extend along astrocytes (Gerhardt et al., 2003), and ultimately, mature blood vessels are superimposed on the astrocyte meshwork (Figure 1A–C). Because the glial network is present first, and because it resembles the vascular plexus that will later form (Figure 1A), it has been proposed that astrocytes provide a template that guides angiogenesis. Several lines of evidence support this notion (Duan, Takeda, & Fong, 2014; Fruttiger et al., 1996; Gnanaguru et al., 2013; Uemura, Kusuhara, Wiegand, Yu, & Nishikawa, 2006), including a recent study demonstrating that astrocytes are critical for onset of retinal angiogenesis (Tao & Zhang, 2016). However, in this study, the complete removal of astrocytes led to a complete failure of vascular development, leaving open the question of how vessel pattern might develop in the absence of an astrocyte template. Thus, the notion that astrocytes are necessary for vessel patterning remains to be tested.

If astrocytes must be present for vascular development to proceed, then understanding how astrocytes themselves are patterned during development is crucial. The axons of retinal ganglion cells (RGCs), astrocytes, and blood vessels are the principal constituents of the RNFL (Figure 1B). RGCs are the earliest born retinal cell type, and their axons converge on the optic nerve head from across the retina as they course toward the brain. RGC axons exit the retina at embryonic

day (E) 12 in mice (Colello & Guillery, 1990), almost a week before astrocytes are first born (Huxlin et al., 1992). Thus, immature astrocytes migrate among them on their journey into the periphery, following a migration route that roughly parallels axon trajectory (Figure 1C). RGCs are known to influence proliferation of astrocyte precursors (Burne & Raff, 1997; Burne, Staple, & Raff, 1996; Dakubo et al., 2003, 2008; Wallace & Raff, 1999), but how RGC axons influence astrocyte migration remains unclear. In mice lacking RGCs, the astrocyte network is dysmorphic (Edwards et al., 2012), suggesting a developmental interaction between the two cell types, but the mechanism by which this phenotype arises has not been determined. Understanding the specific astrocyte cell-biological functions controlled by RGCs will provide critical insight into the mechanisms that determine astrocyte pattern, and therefore vascular pattern.

In this study, we investigated the cellular mechanisms of retinal neuronal-glial-vascular development. First, we confirmed that astrocytes are required for retinal angiogenesis. Using a genetic strategy to specifically deplete astrocytes shortly after birth via diphtheria toxin, we found dramatic reductions in retinal vascularization and mispatterning of growing vessels induced by loss of the astrocyte template. Next, we examined the relationship between astrocytes and RGCs during development and found selective physical association between migrating astrocytes and RGC axons. We tested the functional role of this RGC–astrocyte interaction using mutant mice with intraretinal axon

guidance defects, and *Math5* knockout mice in which retinal progenitors fail to assume the RGC fate. We found that RGCs are required for astrocytes to fully colonize the retina by providing migrating astrocytes with a directional signal. Consequently, in the absence of RGCs, the center-peripheral orientation of individual astrocytes and their network is lost, and astrocytes accumulate near their source at the optic nerve head. Moreover, the fine-scale spatial pattern established by astrocytes is abnormal when they lack RGC guidance cues. Our results support a model in which RGCs are required for astrocytic colonization of the retina, and that astrocytes are in turn necessary for normal vascular development.

2 | MATERIALS AND METHODS

2.1 | Mice

Mice of both sexes were used for experiments under protocols approved by the Duke and Oregon Health & Sciences University IACUCs. Cre driver lines used were the following: (1) *GFAP:Cre* with the human GFAP promoter driving expression of Cre recombinase (Zhuo et al., (2001) Jax stock 004600); (2) *Pax2:Cre* with the Pax2 promoter driving expression of Cre recombinase (Ohya & Groves (2004); obtained from Joshua Weiner, University of Iowa); and (3) *Six3:Cre* ((Furuta, Lagutin, Hogan, & Oliver, 2000); Jax stock 019755). For Cre-dependent fluorescent protein expression, we used three *Rosa26-CAG-lox-stop-lox* lines: (1) a tdTomato reporter line, *Ai14* (Madisen et al., 2010; Jax stock 007914); (2) a farnesylated GFP (fGFP) reporter line, which targets GFP to the plasma membrane (Rawlins et al., 2009; obtained from Brigid Hogan, Duke University); and (3) the *mTmG* line which drives Tomato in the absence of Cre and GFP in the presence of Cre ((Muzumdar, Tasic, Miyamichi, Li, & Luo, 2007); Jax stock 007576). Astrocyte depletion experiments used conditional diphtheria toxin receptor (cDTR) mice (Buch et al., 2005), in which an loxP-flanked stop signal upstream of the simian EGFR gene has been knocked into the *Rosa26* locus (Jax stock 007900, obtained from Daniel Saban, Duke University). *Math5* knockout mice were as described (Brown, Patel, Brzezinski, & Glaser, 2001). Mice carrying a recombinant chromosome harboring linked *Robo1* null (Long et al., 2004) and *Robo2* floxed alleles (Domyan et al., 2013; Lu et al., 2007) were obtained from Le Ma (Thomas Jefferson University). These mice were crossed to the *Six3:Cre* strain to achieve retina-specific knockout of *Robo* receptors. Because loss of *Robo* signaling in endothelial cells causes retinal vascular defects (Rama et al., 2015), we used reporter crosses to confirm previous reports (Furuta et al., 2000) that *Six3:Cre* is neural retina-specific (data not shown).

2.2 | Diphtheria toxin injections

Diphtheria toxin (DT; Sigma Aldrich D0564) was aliquoted at 500 ng/ μ L and stored at -80°C . For each experiment, a fresh aliquot was thawed and diluted to 16–32 ng/ μ L in sterile PBS. P0 mouse pups were injected intraperitoneally or subcutaneously with 80–100 ng DT solution. P5 pups were injected intravitreally with 0.5–1.0 ng DT.

Littermate controls lacking either the *GFAP:Cre* or *cDTR* transgenes received the same DT dose. For the P5 experiment, an additional control was performed: *GFAP:Cre;cDTR* mice received DT in one eye and a sham injection in the other. Sham-injected eyes were indistinguishable from DT-injected eyes from littermates lacking *Cre* or *cDTR* transgenes (data not shown), so the data from both types of controls were pooled. Only *GFAP:Cre;cDTR* mice with >2 SD reduction in total astrocyte number were included in the astrocyte-depleted group for analysis. *GFAP:Cre;cDTR* pups that did not meet this criterion for astrocyte depletion did not differ from controls on any vascular parameter.

2.3 | Immunohistochemistry

Mice were deeply anesthetized with isoflurane, decapitated, eyes rapidly removed, and immersion fixed in 4% paraformaldehyde for 1.5 hr at 4°C . Retinas were subsequently dissected free of the eye and blocked for 2 hr at room temperature in PBS with 0.03% Triton X-100 (Sigma-Aldrich) and 3% Normal Donkey Serum (Jackson ImmunoResearch). Retinas were incubated with primary antibodies in the same blocking solution at 4°C for 5–7 days, washed 3–4 times with PBS, and then incubated with 1:1000 Donkey secondary antibodies (Jackson ImmunoResearch) for 1 day. Retinas were then washed in PBS and flat mounted by making 4 relieving cuts from the retinal periphery approximately two-thirds of the way to the optic nerve head, mounted on cellulose membrane filters (Millipore HABGO1300), and coverslipped with Fluoromount-G (Southern Biotech).

Primary antibodies used were as follows: rat anti-CD31 (1:100, BD Biosciences 550274); goat anti-GFAP (1:1000, Abcam ab53554); chicken anti-GFP (Life Technologies A10262); mouse anti-neurofilament (1:1000, EMD Millipore MAB1621); rabbit anti-Pax2 (1:200, Covance PRB-276P); rat anti-PDGFR α (1:100, BD Biosciences 558774); guinea pig anti-RBPMS (1:1000, Rodriguez, de Sevilla Muller, and Brecha, (2014)); rat anti-RFP (1:500, ChromoTek 5f8–20); and rabbit anti-Sox9 (1:4000, Millipore AB5535). Alexa 488-conjugated *Griffonia simplicifolia* Isolectin B4 (IB4; 1:100, Life Technologies I21411), a marker of vasculature, was included with primary antibodies.

2.4 | Microscopy and image analysis

Images were acquired on a Nikon A1 confocal laser scanning microscope or Olympus IX81 epifluorescence microscope with $60\times$ oil immersion or $20\times$ air objectives. Images were analyzed in FIJI/ImageJ. For astrocyte density measurements, astrocytes were counted in a semi-automated fashion by thresholding Pax2 fluorescence images, separated touching cells with the Watershed function, and counting cells with the Analyze Particles tool. Retina, astrocyte, and vascular areas were measured by drawing perimeters with the Freehand selection tool. Astrocyte-axon co-localization was manually graded in a binary fashion from Z-projections of images from Pax2- and NF-stained retinas. If any portion of a Pax2-positive nucleus overlapped with an NF-positive axon or fascicles, it was graded as an “axonal astrocyte.” Astrocyte morphometry was performed by fitting ellipses to thresholded images of Pax2 immunostained retinas using the Analyze



Particles tool, and measuring area, aspect ratio, and angle. This automated procedure occasionally fit an ellipse to a small cluster of cells instead of a single cell, but such instances were rare and the resulting ellipse generally matched the orientation of the enclosed cells. The angle of the ray defining the center–periphery axis was calculated from XY coordinates of the optic nerve head and of the field of view. Mean angular deviation and angular coherence were calculated using circular statistics with an angle doubling correction to eliminate directionality of orientations. The sine and cosine of each doubled angle was found, the arithmetic mean of sine and cosine calculated, and those values plotted as X–Y coordinates to produce a point on the perimeter of a unit circle. The angle from the origin to that point was taken as the average angle and its distance from the origin, which ranges from 0 to 1, as the angular coherence. Vessel length and capillary loops were measured using the Angiogenesis Analyzer plugin.

For spatial regularity/mosaic analysis, we focused on midperipheral retina because the far periphery is mostly devoid of astrocytes in *Math5* mutants and the central retina contains many astrocytes that completely failed to migrate, which might be qualitatively different from those that successfully reached midperiphery. The density recovery profile, Voronoi domain regularity index, and astrocyte cell diameter were calculated as described (Kay, Chu, & Sanes, 2012; Raven, Eglen, Ohab, & Reese, 2003; Rodieck, 1991). Random simulations were performed as described (Wang et al., 2016) and were separately matched to control and mutant astrocyte density, because mutant density was higher. Note that *Math5* mutant astrocytes in the “Type I” configuration were not subjected to regularity indexing or exclusion zone size calculations because these analyses are not designed to describe arrays displaying local attraction.

2.5 | Data analysis

Data from four images at each eccentricity per retina were averaged for measurements of astrocyte number, astrocyte orientation, astrocyte network morphometry, vessel density, and capillary loop density. Statistical analyses were performed in JMP 12 (SAS Institute). Descriptive statistics are mean \pm SEM, and error bars on graphs are SEM. Student's *t* tests or ANOVAs (one-way or multifactor) with post-hoc *t* tests were used to test significance ($\alpha = 0.05$) as determined by the number of conditions, unless otherwise indicated.

3 | RESULTS

3.1 | Astrocytes are required for normal retinal vascularization

To test the hypothesis that astrocytes form a template that is required for normal retinal angiogenesis, we sought a method to deplete astrocytes during early postnatal development. To do this, we took advantage of the conditional diphtheria toxin receptor (cDTR) mouse line (Buch et al., 2005), which drives DTR expression and hence diphtheria toxin (DT) susceptibility in a Cre-dependent manner. These were crossed to a *GFAP:Cre* driver line to selectively confer DT sensitivity on

astrocytes. We first validated the specificity of the *GFAP:Cre* line by crossing it to fluorescent protein reporter strains. This cross demonstrated that nearly all retinal astrocytes had undergone recombination before postnatal day 1 (P1) (Figure 2A,C). Furthermore, tdTomato expression was not observed in retinal cells outside the RNFL (Figure 2B), or ahead of the wavefront of astrocyte migration within the RNFL (Figure 2A), indicating that recombination had not occurred in neural progenitors or other retinal cell types. While Müller glia of the inner nuclear layer can become labeled by this Cre line in older animals (data not shown), we verified in cross-sections that astrocytes are the only retinal cell type in which this *GFAP:Cre* mouse line drives recombination during the time-frame of our experiments (Figure 2B).

To ablate astrocytes at the beginning of vascular development, we injected *GFAP-Cre; cDTR* mice and control littermates with DT at P0. We then immunostained for astrocytes at P4, finding that astrocyte density was markedly reduced across the entire retina (Figure 2D,F; main effect of genotype, $F(1,39) = 110.1$, $p < .0001$; main effect of eccentricity, $F(2,39) = 57.6$, $p < .0001$; genotype by eccentricity interaction, $F(2,39) = 1.7$, $p = .2050$). We calculated the total number of astrocytes in each retina, and found a 70% absolute reduction in astrocyte number in depleted retinas compared to controls (Figure 2G; control, $21,505 \pm 514$, $n = 10$; depletion, $6,455 \pm 769$, $n = 5$; $p < .0001$). This large reduction in astrocyte number also led to reduced retinal area covered by astrocytes in depleted retinas (Figure 2E,H; control, $93.05 \pm 1.00\%$, $n = 10$; depletion, $66.72 \pm 5.39\%$, $n = 5$; $p = .0073$). Within regions covered by astrocytes, the glial honeycomb-like network was sparse, with larger lacunae and thinner septae than in controls (Figure 2I). We confirmed the selective effect of DT on astrocytes by labeling RGCs with anti-RBPMS and all nuclei with Hoechst. No tissue damage or pyknosis was evident, and cell densities in the ganglion cell layer were similar between *GFAP-Cre; cDTR* mice and littermate controls (Figure 2J).

As we hypothesize that astrocytes form a template that guides angiogenesis, we predicted that retinal angiogenesis in astrocyte-deficient mice would be impaired. To examine the effect of astrocyte depletion on vascular development, we stained control and astrocyte-depleted retinas with anti-CD31 or IB4. These markers label both patent vessels and immature endothelial tip cells (Gerhardt et al., 2003; Figure 3A). In ablated retinas, the spread of endothelial cells away from the optic nerve head was severely impaired; retinal area covered by vasculature at P4 was reduced by 71% relative to controls (Figure 3C; control, $39.3 \pm 1.6\%$, $n = 10$; astrocyte depleted, $11.3 \pm 4.1\%$, $n = 5$; $p = .0011$). Even within the vascular zone, the morphology of the blood vessel network appeared abnormally sparse (Figure 3B). To further probe this idea, we measured the density of capillary loops. We found an 88% decrease in loop density upon astrocyte depletion, demonstrating a significant reduction in the complexity of the vascular plexus (Figure 3D; control, $698 \pm 46 \text{ mm}^{-2}$, $n = 10$; astrocyte depleted, $87 \pm 29 \text{ mm}^{-2}$, $n = 5$; $p < .0001$). To capture the effects of both phenotypes, we created an overall index of retinal angiogenesis by calculating the total length of retinal vessels. This was computed as the vessel density of central retina multiplied by the vascularized retinal area. By

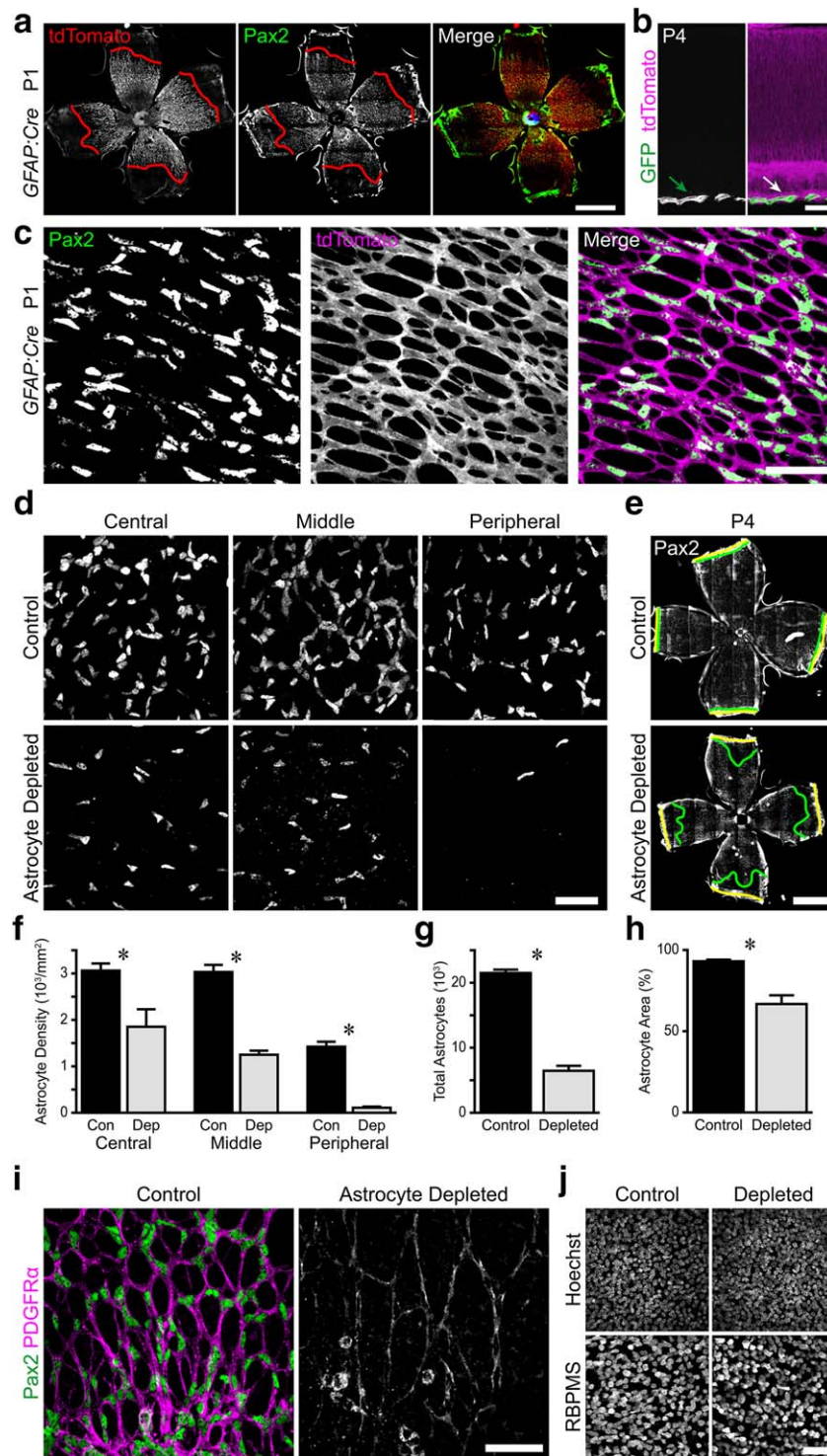


FIGURE 2 Specific depletion of astrocytes during early postnatal development by diphtheria toxin. A–C, Selective expression of *GFAP-Cre* in astrocytes. Composite tile-scan epifluorescence (A) and confocal (C) images from P1 *GFAP-Cre; Ai14* (tdTomato) reporter mouse retinas immunostained for Pax2 and tdTomato. A, tdTomato and Pax2 wavefronts (red lines) align at P1, indicating that recombination occurs in immature astrocytes. C, The entire astrocyte network is labeled with tdTomato, indicating recombination in virtually all astrocytes by P1. B, Cross-section of P4 *GFAP-Cre; mTmG* retina. Unrecombined cells, tdTomato; recombined cells, GFP. Only astrocytes in RNFL (arrow) are GFP+. D, E, Representative images of Pax2 stained *GFAP-Cre; cDTR* (astrocyte depleted) animals and littermate controls lacking DTR expression. All mice were injected with DT at P0 and sacrificed at P4. Yellow lines: retinal edge. Green lines: Pax2 wavefront. F–H, Quantification of astrocyte depletion. Depleted retinas showed reduction in astrocyte density (F), overall number (G), and retinal coverage (H). I, Representative images from the retinal midperiphery illustrating the sparse astrocyte network in depleted retinas. J, Confocal Z-projections through the ganglion cell layer of control and astrocyte-depleted retinas stained with Hoechst and anti-RBPMS to label all nuclei and RGCs, respectively. Cell densities were similar and no pyknotic nuclei were evident, confirming that DT was not killing other retinal cell types. Scale bars: A, E, 1 mm; B, C, D, I, J, 50 μ m [Color figure can be viewed at wileyonlinelibrary.com]

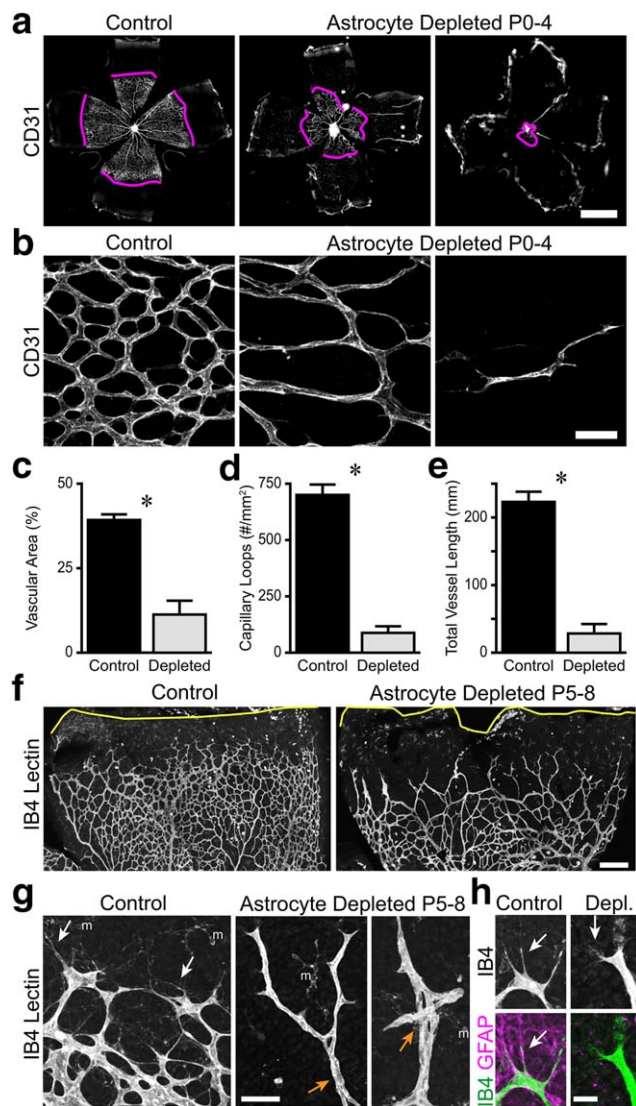


FIGURE 3 Angiogenesis is impaired in astrocyte-depleted retinas. A–E, GFAP-Cre; cDTR mice were injected with DT at P0 to selectively kill astrocytes and analyzed at P4. A,B, Low- (A) and high- (B) magnification images of CD31-labeled vasculature. Magenta lines: vascular wavefront. Vascular coverage of the retina was reduced in astrocyte-depleted retinas (A,C). Density of capillary loops, a measure of vascular complexity, was also reduced (B,D). Total vessel length per retina in astrocyte-depleted animals was significantly smaller than controls (E). F–H, Injection of DT at P5 to selectively kill astrocytes during angiogenesis. Central retina is down and peripheral is up in all images. Low-magnification view of IB4-labeled vessels (F) shows retarded vascular wavefront (also see Results for quantification) and mispatterning of vessels at wavefront of depleted retinas. Capillary loops behind wavefront are also affected. Yellow line, retina edge. High magnification view of wavefront (G) shows patterning errors in depleted mice including reduced capillary looping, abnormal vessel crossings (orange arrows), and lack of filopodia and/or fine branch extensions (white arrows). m, microglial cells labeled by IB4. H, Altered filopodia morphology in astrocyte-depleted animals. At control wavefront filopodia are long, sturdy, and follow GFAP⁺ astrocyte template. In depleted retina lacking GFAP⁺ template, filopodia become shorter and smaller caliber fine protrusions (arrow). Scale bars: A, 1 mm; B, 50 μ m; F, 200 μ m; G, 50 μ m; H, 20 μ m [Color figure can be viewed at wileyonlinelibrary.com]

this measure, retinal angiogenesis was diminished by 87% in astrocyte depleted retinas (Figure 3E; control, 223 ± 15 mm, $n = 10$; astrocyte depleted, 28 ± 13 mm, $n = 5$; $p < .0001$). This experiment thus demonstrates that astrocytes are necessary for vascular development.

Taken together with observations that blood vessels grow along a preexisting astrocyte meshwork (Gerhardt et al., 2003) (Figure 1B) and that endothelial tip cells still follow residual astrocytes in depleted retinas (data not shown), these results support the proposal that astrocytes form a template which is required for retinal angiogenesis during development. However, absence of astrocytes might also impair endothelial cell proliferation, morphogenesis, or other processes necessary for vessel formation. Furthermore, ablation of astrocytes prior to the arrival of endothelial cells leaves open the possibility that the astrocyte template is necessary for initiation but not progression of retinal angiogenesis. For these reasons, we next ablated astrocytes at P5, while vascular colonization of the retina was already underway, and analyzed vessel morphology at P8. Whereas control vessels had nearly reached the retinal edge by this age, the vascular wavefront was generally located in midperiphery of astrocyte-depleted retinas (Figure 3F), leading to a significant reduction in vascularized retinal territory ($87.5 \pm 2.2\%$ vascularized in controls vs $68.0 \pm 2.3\%$ in depleted retinas, $n = 7$ control and 3 depleted, $p < .001$ by two-tailed *t* test). Furthermore, astrocyte removal produced striking morphological changes at the advancing vascular wavefront. One particularly notable phenotype was the near-complete absence of the long, exploratory filopodia that extended exuberantly from tip cells at the wavefront in controls (Figure 3G,H). Upon closer examination, we found that filopodia were not in fact eliminated in depleted retinas, but they significantly changed their morphology—they became far finer and more diffuse in the absence of an astrocyte template, suggesting a reduced rate of exploration and/or migration (Figure 3H). A second notable phenotype was that wavefront vessels tended to be long and unbranched in the absence of astrocytes and frequently adopted abnormal trajectories, such as intertwining with adjacent vessels or self-crossing to form knotted structures (Figure 3G). As in the P0–P4 experiment, far fewer capillary loops were noted at the wavefront of depleted retinas (Figure 3G). By contrast, in central regions presumably vascularized prior to ablation, loops were plentiful, although their variable size suggests that astrocytes may have a role in maintenance of vessels in addition to their initial formation (Figure 3F). Together, these observations indicate that removal of the astrocyte template during vessel development causes severe vascular patterning errors at the advancing wavefront. We conclude that astrocytes provide guidance cues to growing vessels that are essential for retinal angiogenesis.

3.2 | Astrocytes are selectively associated with axons

Given the importance of astrocytes for vessel patterning, we next turned to the question of how astrocytes are patterned during development. A key step in astrocyte patterning is their migration to colonize peripheral retina. As the axons of RGCs are already present in the RNFL when astrocytes begin their migration, they are well positioned to guide migrating astrocytes from the optic nerve head to the periphery (Figure 1C). As an initial test of this idea, we asked whether

astrocytes physically interact with RGC axons as they migrate. We imaged the RNFL in flat-mounted retinas immunostained for neurofilament to mark RGC axons and Pax2 to specifically label astrocyte nuclei. At P1, during their migration, astrocyte nuclei appeared tightly associated with RGC fascicles, whereas at P7, when migration is complete, there was no longer any obvious morphological coupling between the two cell types (Figure 4A). This observation suggests that astrocytes selectively associate with axons during their migratory phase. In

support of this idea, we found that the vast majority (~75%) of P1 astrocytes were in contact with axon fascicles (Figure 4C,D).

We considered the possibility that this high contact rate might arise by chance—i.e., through the coincidental superposition of two structures that are in fact independently distributed. However, two lines of evidence favor the notion that the interaction is in fact selective. First, we tested for selective interactions by taking advantage of the fact that the RNFL territory occupied by RGC axons varies with

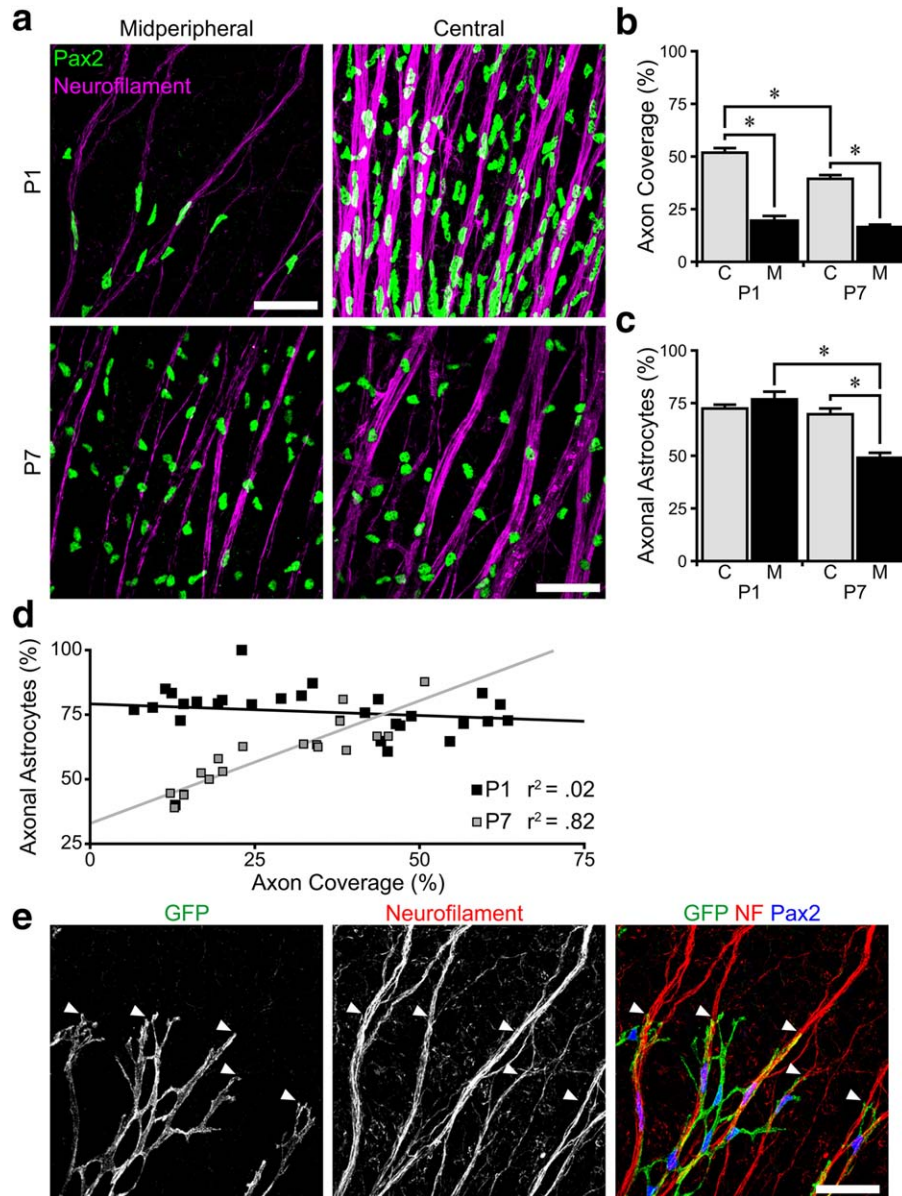


FIGURE 4 Astrocytes selectively associate with axon fascicles during migration. A, Flat-mount P1 and P7 retinas stained for RGC axons (neurofilament) and astrocytes (Pax2), imaged in central and midperipheral retina. Astrocyte nuclei conform to axons at P1, but not at P7. B, C, Quantification of the area of the RNFL covered by axons (B) and the percentage of astrocyte nuclei that localize on axon fascicles (C) in central (C) and midperipheral (M) retina. While axonal coverage decreases dramatically in midperiphery, axonal astrocyte localization is high in both regions at P1. At P7, astrocytes are less frequently found on axon fascicles in the midperiphery where there are fewer fascicles. D, Scatter plot of axon coverage versus axonal astrocyte localization for each field of view across all eccentricities. At P1, there is no correlation between coverage and colocalization, suggesting that astrocytes selectively associate with axons. At P7, there is a strong correlation between coverage and colocalization, suggesting that astrocyte–axon colocalization is coincidental. E, Pax2-Cre;fGFP mice label a subset of astrocytes with GFP. At P1, GFP-labeled astrocyte leading processes colocalize with RGC axon fascicles (neurofilament, NF) at the astrocytic wavefront (arrowheads). Scale bar: 50 μ m [Color figure can be viewed at wileyonlinelibrary.com]



eccentricity: Because RGC axons converge at the optic nerve head, RGC axons cover more of the RNFL in central retina than in the mid-periphery (Figure 2A,B; main effect of eccentricity, $F(1, 47) = 120.7$, $p < .0001$). If colocalization of astrocyte nuclei and RGC axons were coincidental, we would also expect a higher colocalization rate in central retina where axons are more abundant. However, astrocytes at P1 contact axons at similarly high rates in the central and midperipheral retina, suggesting that the interaction is selective (Figure 4C). Indeed, when we directly examined the relationship between colocalization rate and axon territory across all eccentricities, we found that these two parameters were not related at P1 (Figure 4D). By contrast, the same analysis performed at P7 shows the opposite: Astrocyte colocalization rate and axon territory are highly correlated once astrocytes have finished migrating (Figure 4B–D), suggesting that any apparent associations are coincidental. Second, as a direct test of specific astrocyte–axon interactions, we visualized the morphology of migrating astrocytes by crossing conditional membrane-targeted fGFP reporter mice with a *Pax2:Cre* BAC transgenic line that drives fGFP expression in a subset of developing astrocytes. This labeling revealed that astrocytes were intimately associated with axon fascicles at P1, and that the leading processes of astrocytes at the wavefront selectively extended along axon bundles (Figure 4E). Together, these observations indicate that astrocytes specifically accumulate on RGC axons during their migration, but they no longer do so when migration is complete.

3.3 | Ganglion cell axons are sufficient to orient migrating astrocytes

As astrocytes selectively associate with RGC axons during the migratory phase of their development, we supposed that RGCs might guide astrocyte migration. If this is true, astrocytes should follow RGC axons even if they adopt abnormal trajectories. To test this hypothesis we examined mutant mice lacking Roundabout (*Robo*) receptors. Deletion of *Robo2*, or its Slit family ligands, causes RGC axons of peripheral retina to travel long distances in the circumferential axis, orthogonal to the centripetal course of wild-type RGCs (Thompson, Andrews, Parnavelas, & Erskine, 2009; Thompson, Camand, Barker, & Erskine, 2006). Some mutant RGC axons also exit the RNFL and dive to deeper retinal layers. Because these axon trajectories differ starkly from the normal astrocyte migration path, they offer an opportunity to ask whether axon trajectory is sufficient to guide migrating astrocytes. Germline *Robo2* mutants die at birth, prior to astrocyte migration, so we used a conditional strategy to generate viable retina-specific knockouts (rKOs). We crossed the retinal progenitor-specific *Six3:Cre* line to double mutant mice bearing a *Robo1*[−] null allele and a *Robo2*^{fllox} conditional allele, thereby generating *Robo1/2*^{rKO} mice. *Robo1/2*^{rKO} animals were born at expected ratios and survived to adulthood. Overall retinal histology was not obviously perturbed, and RGCs were present in normal numbers (Figure 5B,C).

Neurofilament staining of postnatal *Robo1/2*^{rKO} animals revealed axon guidance phenotypes similar to those reported for embryonic retina (Thompson et al., 2006). In littermate controls (double-heterozygous mice and cre-negative *Robo1* single mutants), RGC axons reliably

oriented along the center–peripheral axis (Figure 5A). In mutants, while axon trajectories were mostly normal in central retina, peripheral axons showed striking errors that included looping structures and circumferentially oriented axon fascicles (Figure 5A). Axon projections to deeper retinal layers were also observed (not shown). To ask if axons can orient astrocytes, we examined the association of Pax2⁺ nuclei with RGCs in *Robo1/2*^{rKO} mutants. Astrocytes did not leave the RNFL to enter deeper layers in mutants, consistent with their affinity for the extracellular matrix of the inner limiting membrane (Gnanaguru et al., 2013). However, when axons made circumferential errors within the RNFL, astrocytes remained tightly associated with these axons and elongated their nuclei along them (Figure 5D; $n = 4$ mutants and 3 littermate controls). The association of *Robo1/2*^{rKO} astrocytes with axons was similar to that observed in littermate controls (Figure 5D) and wild-type mice (Figure 4A), suggesting that the axis along which astrocytes formed chains and polarized their nuclei was dictated by the orientation of the associated axons. Thus, RGC axons appear capable of providing directional cues to migrating astrocytes that influence their orientation.

3.4 | Ganglion cells are required for astrocytic colonization of the retina

To test whether these axon-derived directional cues are required for dispersal of astrocytes into peripheral retina, we next examined astrocytes in *Math5* null mice. The *Math5* gene encodes a transcription factor transiently expressed by retinal progenitor cells that is required for RGC fate specification (Brown et al., 1998, 2001; Wang et al., 2001). Very few RGCs differentiate in the absence of *Math5* (Figure 6A,B), but other major cell types are present and retinal cytoarchitecture is largely normal (Brown et al., 2001; Wang et al., 2001; C. Kozlowski & J.N.K., unpublished observations). Consistent with a previous report using a different *Math5* mutant line (Edwards et al., 2012), we found that intrinsic retinal vasculature was absent until P7. By the second postnatal week, variable and disorganized vessels were found at the retinal surface (Figure 6C), likely corresponding to neovascularization derived from persistent hyaloid vessels rather than true intrinsic retinal vasculature (data not shown; Edwards et al., 2012). These vascular phenotypes in *Math5* mutants hint at an underlying deficit in astrocyte development. Indeed, using antibodies against the cytoskeletal protein GFAP, it was noted that the astrocyte network has abnormal morphology (Edwards et al., 2012), raising the possibility that migration might be affected. However, the absence of RGCs could influence astrocyte development in a number of ways to produce the described phenotypes.

To specifically test the influence of RGCs upon astrocyte migration, we used the nuclear marker Pax2 to track the position of individual cells as they colonized the *Math5* mutant retina during early postnatal development. In littermate controls, Pax2⁺ astrocytes covered approximately half the retina by P1, and the percentage of the retina covered by astrocytes increases with age (Figure 6D–F; main effect of age, $F(3,27) = 91.2$, $p < .0001$). Migration is completed between P4 and P7. In contrast, the area of retina covered by astrocytes is reduced in *Math5* knockouts, with larger deficits seen at the earliest ages (Figure 6D–F; main effect of genotype, $F(1,27) = 174.3$,

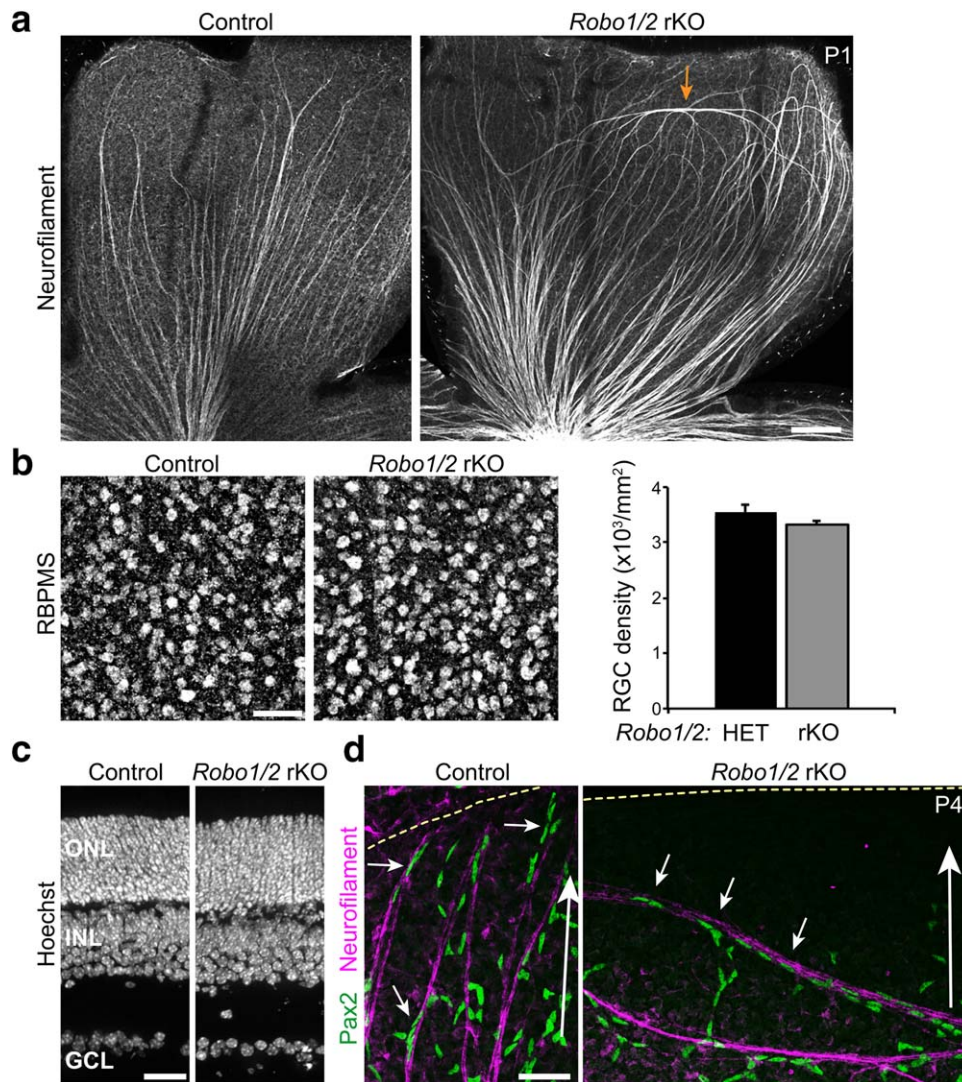


FIGURE 5 Abnormal astrocyte orientation in RGC axon guidance mutants. **A**, Composite tile-scan confocal images illustrating RGC axon phenotype in mice with a retina-specific knockout (rKO) of Robo receptors. In littermate controls, neurofilament-labeled axon fascicles run exclusively along the center–peripheral axis (center is down and peripheral is up in both panels). In *Robo1*^{-/-}; *Robo2*^{fl/fl}; *Six3:Cre* (*Robo1/2* rKO) animals, axons in central retina are normal, but in peripheral retina some axons run along the circumferential axis (arrow). **B**, The number of RBPMS+ RGCs is normal in *Robo1/2* rKO mice (P7). Left, whole-mount confocal images; right, cell counts. **C**, Overall retinal morphology, assessed in cross-section using Hoechst nuclear stain, is not affected by loss of Robo1 and Robo2 (P21). ONL, outer nuclear layer; INL, inner nuclear layer; GCL, ganglion cell layer. **D**, Orientation of Pax2+ astrocytes along axons in littermate control and *Robo1/2* rKO retinas. Large white arrow indicates center–peripheral axis; yellow dashed line denotes retinal edge. Astrocyte nuclei tightly associate with axons and are elongated along the axon fascicle (small arrows), regardless of whether axons travel along the normal centrifugal trajectory (control, left), or orthogonal to the normal trajectory (rKO, right). Scale bars: A, 100 μm ; B,D, 50 μm ; C, 25 μm [Color figure can be viewed at wileyonlinelibrary.com]

$p < .0001$; interaction, $F(3, 27) = 10.9$, $p = .0002$). Though astrocytic territory does expand in knockouts, even by the end of the second postnatal week astrocytes have failed to enter some regions of peripheral retina. These experiments demonstrate that without RGCs, there is a defect in astrocyte colonization of the retina.

3.5 | Ganglion cell axons provide a directional cue for astrocyte migration

To understand how the interaction between RGC axons and migrating astrocytes might facilitate the spread of astrocytes across the RNFL,

we next investigated the nature of the errors made by astrocytes in *Math5* mutants. Given that astrocytes can move away from their central point of origin in mutants, albeit imperfectly, we surmised that migratory ability *per se* is not impaired. Instead, based on our observations in *Robo1/2*^{CKO} animals, we hypothesized that axon-derived cues are required to orient migrating astrocytes along the center–peripheral axis. To investigate this possibility, we examined the shape and orientation of astrocyte nuclei in wildtype and *Math5* null retinas by Pax2 staining (Figure 7A). Astrocytes were analyzed by fitting ellipses to Pax2+ nuclei and measuring their elongation (aspect ratio) and cell-to-cell consistency of orientation (angular coherence). Early in

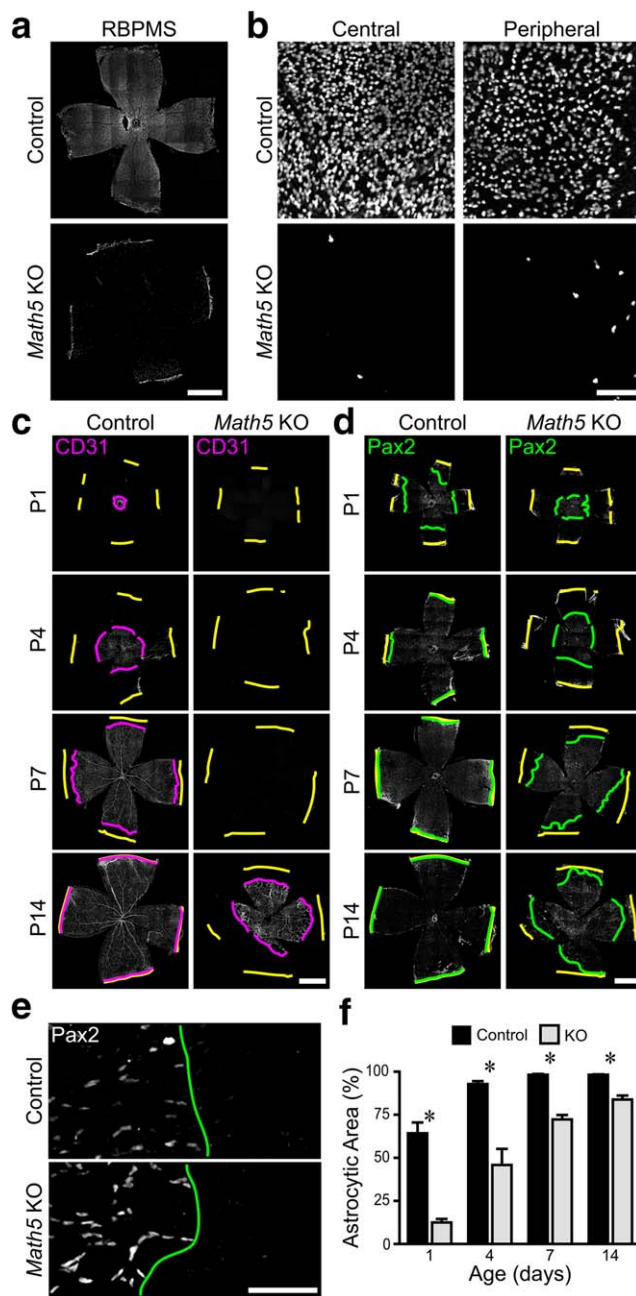


FIGURE 6 RGCs are required for colonization of the retina by astrocytes. A,B, P7 *Math5* knockout and control retinas were immunostained for RBPMS, a pan-RGC marker. Composite tile-scan (A) and high-magnification (B) confocal images of control and knockout retinas. RBPMS-positive cells are nearly absent from knockout retinas. C,D, Composite tile-scan confocal images of flat-mounted control and *Math5* null retinas immunostained for vasculature (CD31; C) or astrocytes (Pax2; D). Yellow lines: retinal edge. Magenta and green lines: CD31 and Pax2 wavefronts. Intrinsic retinal vasculature is absent until P14 (C). E, Higher magnification images from tile-scans (P1) illustrating how lines were drawn at the clear boundary between central astrocytic and peripheral astrocyte-free zones. F, Quantification of retinal area covered by astrocytes across development in controls and *Math5* knockouts. Astrocytic territory is reduced and expansion delayed in knockouts. Scale bars: A,C,D, 1 mm; B,E, 100 μ m [Color figure can be viewed at wileyonlinelibrary.com]

development, wild-type astrocyte nuclei were highly elongated, reflecting their migratory state; their aspect ratio dropped significantly over the course of the first postnatal week as they finish migrating (Figure 7B; main effect of age $F(3,95) = 63.5$, $p < .001$). This general pattern was also seen in *Math5* knockouts, but nuclei were less polarized at younger ages (Figure 7A,B; main effect of genotype, $F(1,95) = 31.7$, $p < .001$; age by genotype interaction, $F(2,95) = 10.1$, $p < .001$), implying that immature astrocytes may be more likely to stop migrating, or to migrate in an undirected manner, in the absence of RGCs. To test whether the orientation of astrocytes depends on the presence of RGCs, we measured the angular coherence of local populations of astrocytes. In controls, the orientations of astrocytes were highly aligned at P1; most cells were polarized along the centrifugal axis (Figure 7A,C). As they completed their migration over the first postnatal week, alignment correlation diminished (Figure 7C; main effect of age, $F(3,95) = 35.6$, $p < .001$). By contrast, in the absence of RGCs, astrocyte orientations were essentially uncorrelated at all ages, suggesting that each migrating cell adopted its own distinct trajectory (Figure 7C; main effect of genotype, $F(1,95) = 76.7$, $p < .001$; age by genotype interaction, $F(2,95) = 13.9$, $p < .001$). We also compared the cellular morphology of astrocytes in wildtype and *Math5* knockout retinas using *Pax2:Cre; fGFP* mice. At P1, astrocytes are normally elongated along the center-peripheral axis, with thin trailing and leading processes and few side branches (Figure 7D). In contrast, astrocytes in *Math5* null retinas are shorter and broader with more abundant branches (Figure 7D). These data show that RGCs are required for proper centrifugal polarization of migrating astrocytes.

We wondered if this failure in astrocyte direction-finding during migration could explain our observation that astrocytes fail to reach the retinal periphery in *Math5* mutants (Figure 6). In the absence of RGCs as orientation cues, astrocyte migration might be undirected and inefficient, leading to accumulation of astrocytes in central retina and fewer reaching the periphery. To test this idea, we investigated how astrocyte density evolved over time at different retinal eccentricities (Figure 8A). In P1 controls, astrocyte density is highest near the optic nerve head, and density declines with eccentricity (Figure 8B,C). With increasing age, central densities fall while peripheral densities increase, such that a homogeneous astrocyte density distribution across the retina is achieved by P7 (Figure 8B-D). In *Math5* knockouts, by contrast, the peak of astrocyte density in central retina is reached late, at P4, and peripheral densities increase only slowly with age (Figure 8B,C). When we plotted the slope of the astrocyte density gradient over time (Figure 8D), it became clear that *Math5* knockouts preserve an abnormally steep center-to-peripheral gradient across development (main effect of age, $F(3,26) = 17.2$, $p < .0001$; main effect of genotype, $F(1,26) = 53.6$, $p < .0001$; age by genotype interaction, $F(3,26) = 47.0$, $p < .0001$).

To understand why the gradient remained steep in mutants, we asked whether mutants have higher astrocyte density centrally, lower density peripherally, or both. To this end, we used three-way ANOVA to test for effects of genotype on local cell densities. We found

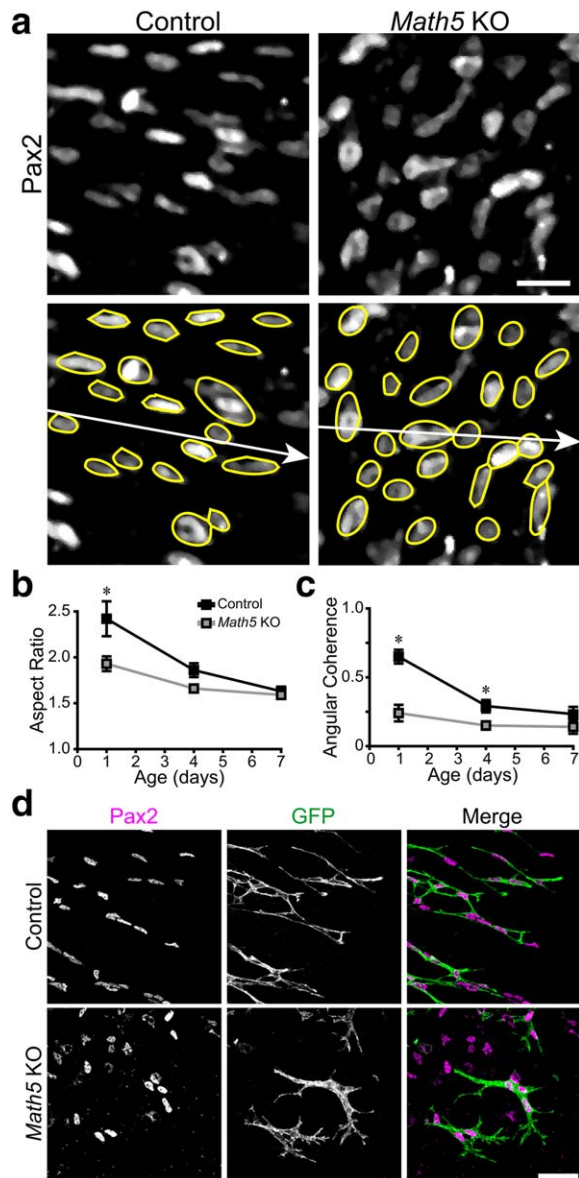


FIGURE 7 Ganglion cells are necessary for astrocyte polarization along the centrifugal retinal axis. **A**, P1 retinas were stained with Pax2 to label astrocyte nuclei, and astrocyte nuclei were fit with ellipses (yellow) for analysis. **B,C**, Analysis of elongation (**B**) and angular coherence of elongated astrocytes (**C**). In controls, P1 astrocytes were elongated parallel to the ray extending outwards from the optic nerve head to the ora serrata (white arrow in **A**). Both elongation and coherence diminished at later ages after migration was complete. In *Math5* mutants, P1 astrocytes were less elongated (**B**) and their orientations were randomized (**C**), similar to postmigratory wild-type astrocytes. **D**, Morphology of Pax2-Cre;fGFP⁺ astrocytes in control and *Math5* mutant retinas at the P1 astrocyte migration wavefront. Central retina is to the left and peripheral is right in these panels. Similar to their nuclei, control astrocytes were elongated centrifugally. In contrast, knockout astrocytes were broader and less coherently organized along the centrifugal axis. Scale bar: 50 μm [Color figure can be viewed at wileyonlinelibrary.com]

significant main effects of age ($F(3,80) = 14.4, p < .0001$), genotype ($F(1,80) = 4.7, p = .0335$), and eccentricity ($F(2,80) = 109.2, p < .0001$), and all interactions were significant (age by genotype interaction, F

(3,80) = 16.8, $p < .0001$; age by eccentricity interaction, $F(6,80) = 6.5, p < .0001$; genotype by eccentricity interaction, $F(2,80) = 18.1, p < .0001$; age by genotype by eccentricity interaction, $F(6,71) = 17.4, p < .0001$). A key finding was that P4–7 mutants had both an abnormally high astrocyte density in central retina and an abnormally low density in peripheral retina (Figure 8C), suggesting that astrocytes are retained near their origin at the optic nerve head and only rarely reach the periphery. Central density was elevated despite the fact that mutants have fewer astrocytes overall at this age (Figure 8E,F; main effect of age, $F(3,26) = 28.0, p < .0001$; main effect of genotype, $F(1,26) = 21.7, p = .0002$; interaction, $F(3,26) = 2.2, p = .1156$). Together, these experiments support the notion that RGCs facilitate astrocyte colonization of peripheral retina by orienting their migration along the proper vector. In the absence of this orienting cue, many astrocytes fail to escape central retina, creating the density gradient we observe here.

3.6 | Ganglion cells regulate local spatial pattern of astrocytes

The ultimate pattern of the astrocyte network depends not only on long-range migration but also on fine-scale cell body organization. As astrocytes are only physically associated with axons during long-range migration, we considered the possibility that, despite initially disoriented migration, astrocytes might be able to achieve their normal soma arrangement in the absence of RGCs. To investigate this question, we examined the spatial pattern of astrocytes in mature (P14) *Math5* mutant and control retinas. Normally, astrocytes form a mosaic (Chan-Ling & Stone, 1991; Distler, Dreher, & Stone, 1991; Tout, Dreher, Chan-Ling, & Stone, 1993)—that is, their cell bodies are nonrandomly spaced, showing evidence of short-range cell-cell avoidance (Figure 9A–C). As a result, astrocyte somata are more regularly spaced across the retina than would be expected by chance (Figure 9D). In the portion of *Math5* mutant retina that contained astrocytes, we noted two types of cell body arrangements that appeared to be categorically distinct. Neither of these patterns, which we call Type I and Type II, resembled the astrocyte distribution in control mice (Figure 9A). Analysis of each pattern with the density recovery profile (DRP; Rodieck, 1991) confirmed that they are indeed distinct spatial patterns (Figure 9B), so we proceeded to characterize them separately. Neither the Type I nor the Type II arrangements were a mosaic. Unlike the control DRP, which shows an exclusion zone of nearly 30 μm around each cell in which another astrocyte is less likely to reside, the mutant DRPs lacked a region of lowered cell density (Figure 9B,C). Instead, the Type I DRP showed a strong propensity for short-range cell-cell attraction, which was evident from the large astrocyte clumps separated by astrocyte-free zones that characterized this arrangement (Figure 9A, B). The Type II DRP, meanwhile, had uniform cell density at all spatial scales, an arrangement indistinguishable from a random distribution of cells (Figure 9B,C). As a result, astrocytes in the Type II pattern were distributed significantly less regularly than control astrocytes (Figure 9D; one-tailed t test, $p < .01$). Thus, whether they

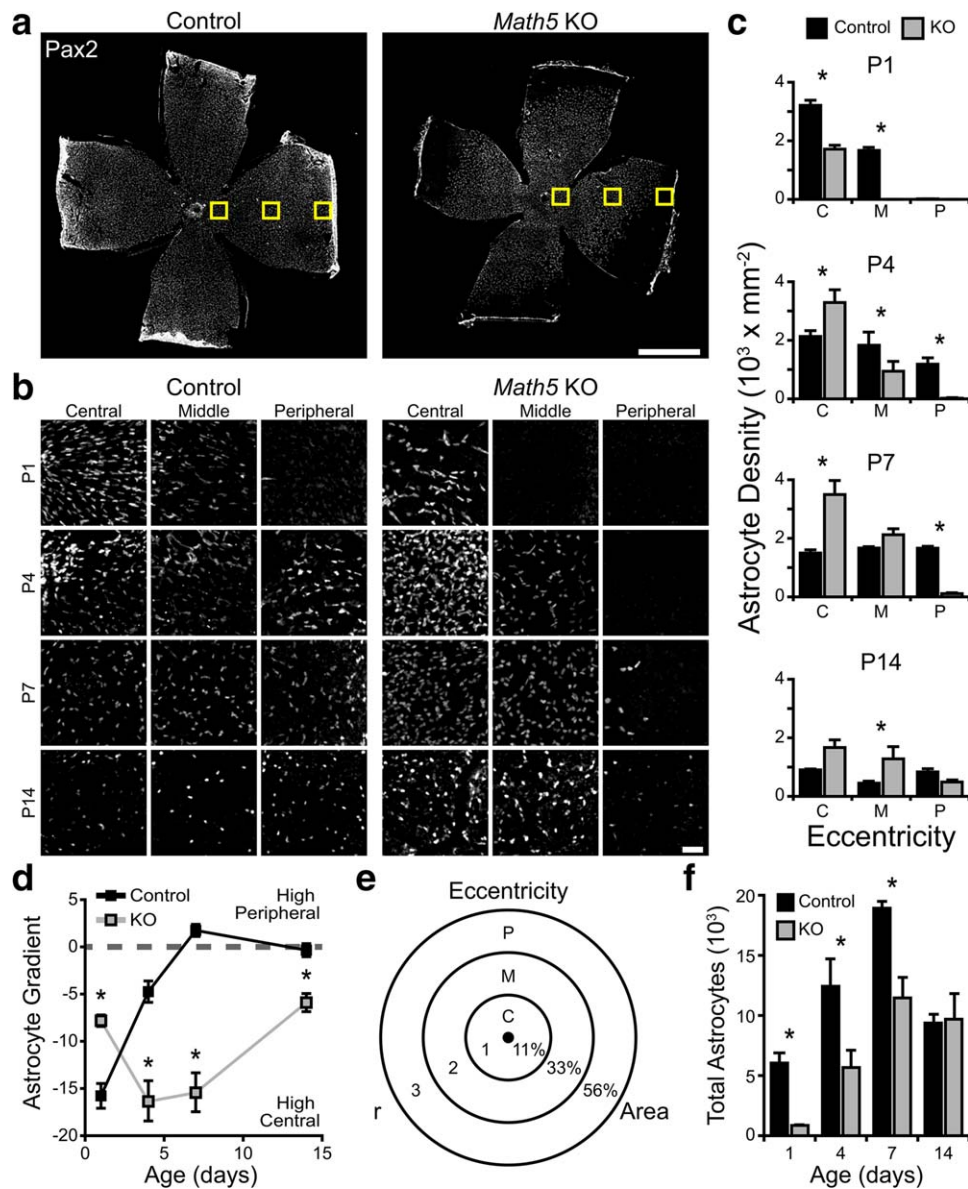


FIGURE 8 Astrocytes accumulate in the center of the *Math5* mutant retina. **A**, Composite tile-scan confocal images of flat-mounted P7 control and *Math5* knockout retinas stained for Pax2 to label astrocytes. Yellow boxes schematically indicate the three eccentricities at which astrocyte density was measured. **B,C**, High-magnification images (**B**) and quantification (**C**) showing astrocyte density in central, midperipheral, and peripheral retina of mutants and controls at four ages. At P4–7, note increased cell density in mutant central retina, and decreased density in peripheral retina, relative to controls. **D**, The three densities measured for each retina were fit with a straight line to produce an astrocyte density gradient for each retina. Negative values denote an outwards gradient, with higher densities of astrocytes in central retina. Dashed line at 0 denotes equal cell density across the retina. Control mice are born with a “high-central” gradient that flattens by P7 as astrocytes move into the periphery. Knockouts show a different developmental trajectory with the gradient first becoming steeper, indicating an accumulation of astrocytes in central retina. **E,F**, Total astrocyte number was estimated from these local densities by measuring retinal area and using a simple model of density distribution in which the retina is divided into 3 zones by circles of expanding radii (**E**). Numbers indicate fraction of total area found in each zone. The calculated total number of astrocytes was reduced in *Math5* null retinas during the first postnatal week, but equalized with controls by P14. Scale bars: **A**, 1 mm; **B**, 50 μm [Color figure can be viewed at wileyonlinelibrary.com]

assume the Type I or Type II configuration, astrocyte spatial pattern is severely perturbed in the absence of RGCs. Upon colabeling with blood vessel markers, we noticed that the Type I arrangement was found only in retinal regions that did not become colonized by neovascularization from the hyaloid vessels (Figure 9A). Our results

therefore suggest that astrocytes deprived of both RGC and vascular contact tend to aggregate into clumps, while those deprived only of RGC contact assume random positions. Alternatively, astrocytes in the clumped Type I pattern may not be capable of promoting angiogenesis.

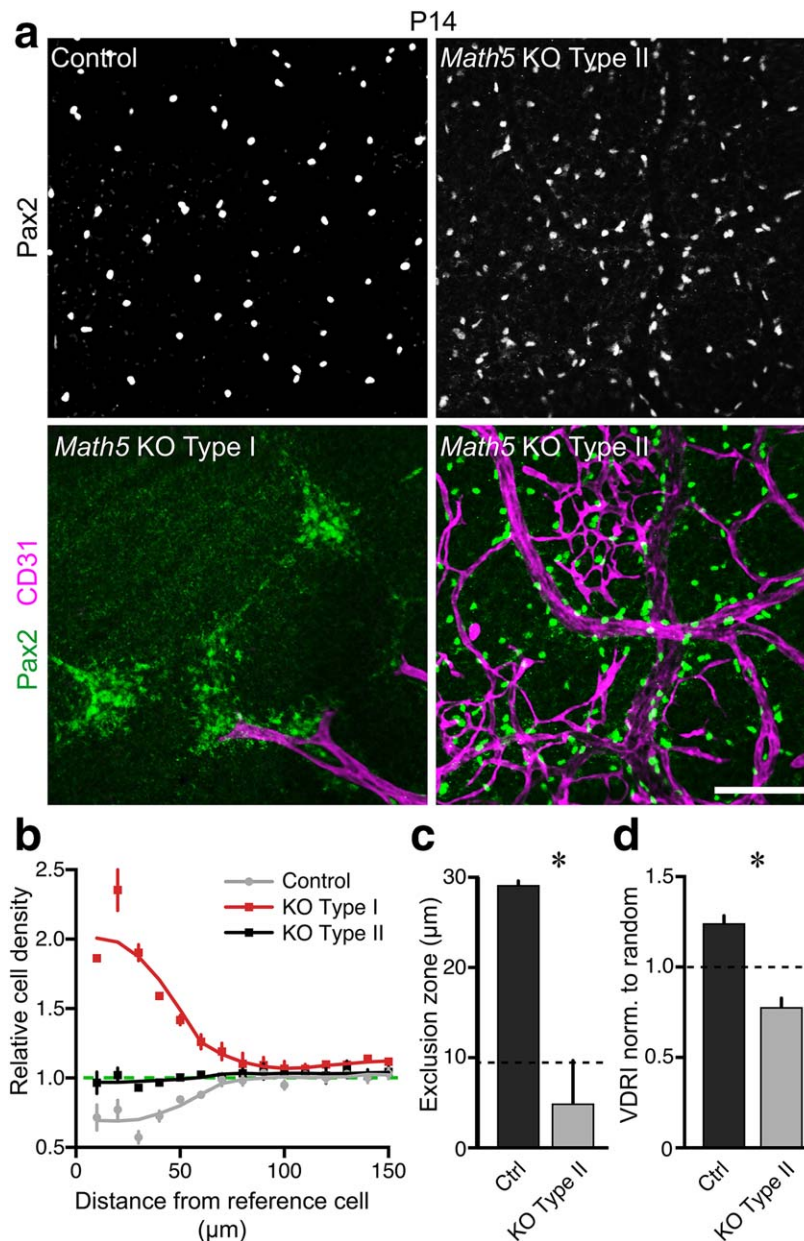


FIGURE 9 Fine-scale astrocyte soma patterning is disrupted in *Math5* mutants. **A**, Astrocyte spatial pattern was assessed in flat-mounted control and *Math5* null retinas stained for astrocyte nuclei (Pax2) and vasculature (CD31). Control astrocytes were evenly spaced. Two types of perturbed patterns were observed in mutants, one strongly correlated with the absence of vasculature (Type I) and the other strongly correlated with presence of vasculature (Type II). The Type I pattern consisted of large, high density patches of astrocytes, separated by astrocyte-free regions. In Type II, astrocytes were more dispersed. **B**, Density recovery profiles (DRPs) of each astrocyte pattern. Inter-cellular distances were computed and binned in annuli of increasing size (10 μm increments). The cell density in each annulus was normalized to the cell density of the entire image. At short intercellular distances, astrocyte density in control mice is lower than the average density (dashed line), indicating the presence of an exclusion zone and hence cell-cell avoidance. In mutant Type I zones, astrocyte density is extremely high at short spatial scales, indicative of aggregation. In Type II mutant regions, astrocyte density matches the overall density (dashed line) at all spatial scales, suggesting that they are randomly distributed. **C**, The exclusion zone, within which another astrocyte was unlikely to be found, was calculated as the DRP effective radius (Rodieck, 1991). Control astrocytes have larger exclusion zones than mutants in the Type II configuration (one tailed *t* test, $p < .01$). Dashed line, average astrocyte cell diameter, which is the expected exclusion zone size for a random array of cells in a plane. The mutant Type II exclusion zone size is similar to cell diameter, consistent with random positioning. By contrast, control astrocytes are a mosaic because their exclusion zone is significantly larger than average soma diameter, indicating local cell-cell repulsion. **D**, Regularity of astrocyte spacing assessed by the Voronoi domain regularity index (VDRI). Data are normalized to VDRI of simulated random arrays. Separate random simulations were performed for control and mutant because their astrocyte density differs in midperipheral retina (Figure 8). Dashed line, expected VDRI for random array. Control astrocytes are significantly more regular than random (one-way ANOVA with post-hoc Bonferroni-corrected test, $p < .0001$). Mutant astrocytes are significantly less regular than random (same test as above, $p < .05$), suggesting that their positioning might be subject to an external force such as blood vessels (A). Scale bar (A) = 100 μm [Color figure can be viewed at wileyonlinelibrary.com]



3.7 | Ganglion cells regulate morphology of the astrocyte network

Upon concluding their migration, astrocytes undergo molecular and anatomical differentiation to assume their mature phenotype. We next examined how RGCs influence this maturation process. Molecular maturation was probed by staining for GFAP, which is expressed at a later point in astrocyte differentiation than Pax2 (Chan-Ling, Chu, Baxter, Weible li, & Hughes, 2009). In wild-type retina, comparing GFAP to Pax2 staining reveals that a wave of maturation follows the arrival of astrocytes to any given retinotopic position by several days, resulting in a center-peripheral gradient of GFAP staining intensity (Figure 10A). In *Math5* mutant retinas, the onset of GFAP expression is delayed, but

GFAP-staining expands rapidly to cover most of the Pax2-positive astrocytic territory by P7 (Figure 10A). Measurement of the retinal area covered by mature, GFAP-positive astrocytes revealed significant main effects of age ($F(3,19) = 3730$, $p < .0001$) and genotype ($F(1,19) = 177$, $p < .0001$), and a significant interaction ($F(3,19) = 18$, $p < .0001$) (Figure 10B). However, when we normalized the GFAP area to the mean area covered by Pax2-positive astrocytes at the same age, the main effect of genotype was no longer significant (main effect of age, $F(3,22) = 3145$, $p < .0001$; main effect of genotype, $F(1,22) = 1$, $p = .31$; interaction, $F(3,22) = 31.74$, $p < .0001$) (Figure 10C). These analyses indicate that the onset of astrocyte molecular maturation is delayed in the absence of RGCs but maturation of the astrocyte population rapidly catches up to control by the end of the first week.

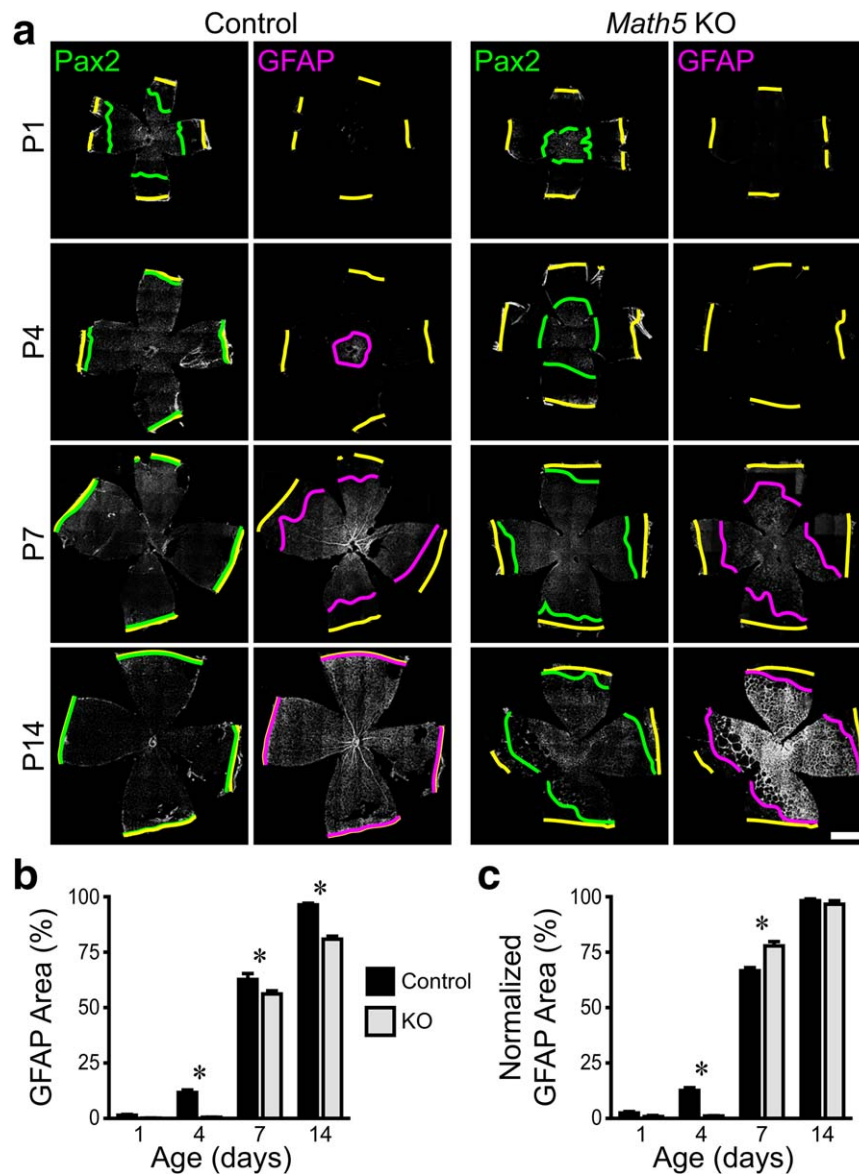


FIGURE 10 Delayed immunohistochemical maturation of astrocytes in *Math5* mutants. A, Composite tile-scan confocal images of flat-mounted control and *Math5* null retinas immunostained for all astrocyte nuclei (Pax2) and mature astrocytes (GFAP). Yellow lines: retinal edge. Green lines: Pax2 wavefront. Magenta lines: GFAP wavefront. B, Quantification of retinal area covered by mature astrocytes across development in controls and *Math5* knockouts. C, Quantification of GFAP area normalized to the mean Pax2 coverage for each condition. Scale bar: 1 mm [Color figure can be viewed at wileyonlinelibrary.com]

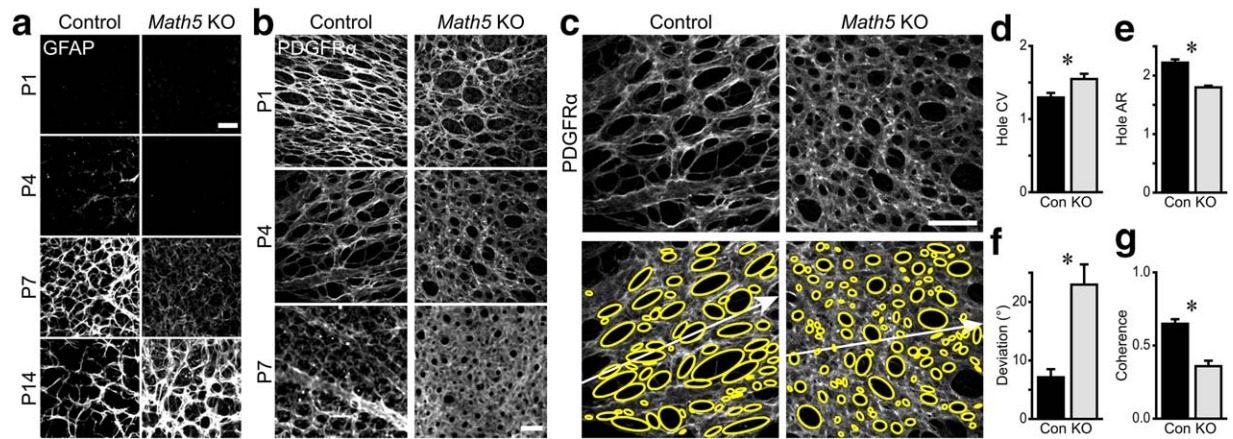


FIGURE 11 Ganglion cells regulate the morphology and polarization of the astrocyte network. **A**, Images from central retina of GFAP-stained control and *Math5* knockout retinas across development. Onset of detectable GFAP protein is delayed in knockouts, but the GFAP network becomes denser and more intensely labeled than controls at P14. **B**, PDGFR α staining reveals morphology of the developing astrocyte network in central retina. In controls, astrocytes form a reticular, honeycomb network with ovoid holes; PDGFR α signal decreases at P7. In mutants, astrocytes form a lawn of increasing density. **C–G**) Astrocyte network morphometry from P4 retinas immunostained for PDGFR α . Ellipses (yellow) were fit to the area devoid of astrocyte coverage. White arrows: ray extending from the optic nerve head to the ora serrata. Morphometric network parameters were altered in the knockout, with holes being more variable in size (**D**), less elongated (**E**), aligned poorly to the centrifugal axis (**F**), and inconsistently oriented relative to each other (**G**). CV: coefficient of variation. AR: aspect ratio. Scale bar: 50 μ m [Color figure can be viewed at wileyonlinelibrary.com]

As astrocytes mature, they assume a stellate morphology to generate their characteristic network in the RNFL. Using GFAP staining, it was previously noted that the morphology of this network is altered in *Math5* mutants (Edwards et al., 2012). For example, the mutant network in central retina appeared sparse relative to controls at young ages but became abnormally dense over time (Edwards et al., 2012; Figure 11A,B). This was initially ascribed to differences in astrocyte density (Edwards et al., 2012), but our data now show that the density of astrocytes in mutant central retina holds steady (from P4–7) and then declines (by P14) during this period of network overelaboration (Figure 8C). This observation prompted us to ask whether astrocyte morphology might also be sensitive to cues derived from RGCs. To address this question, we stained retinas with antibodies to the cell-surface marker PDGFR α , which, unlike GFAP, is expressed by immature astrocytes and labels the complete cell volume. At P1, astrocyte coverage in *Math5* null retinas appeared somewhat sparser than controls, but by P7 astrocytes in mutant central retina had formed a lawn nearly devoid of the normal reticular features of retinal astrocytes (Figure 11B). The phenotype is much more severe than that observed from GFAP staining of the cytoskeleton alone, likely reflecting the cell-surface localization of PDGFR α (Figure 11A).

To better understand changes in the mutant astrocyte network, we developed a set of quantitative morphometric parameters to characterize the regularity and polarization of the network in a manner similar to our approach with astrocyte nuclei (Figure 7A,B). We focused this analysis on P4, when PDGFR α staining was most robust. As astrocytes cover the RNFL with a honeycomb meshwork defined by interspersed astrocyte-free holes (Figure 11B), we began by fitting ellipses to areas devoid of PDGFR α staining (Figure 11C). The ellipses outlining the wild-type astrocyte network were elongated, of similar size, and consistently oriented along the center–peripheral axis. On the other

hand, in *Math5* mutant retinas the ellipses appeared more variable in alignment and size. Morphometry corroborated these observations, with knockouts showing (1) more size variability (Figure 11D; control coefficient of variation $1.29 \pm .06$, $n = 24$; knockout 1.55 ± 0.07 , $n = 26$; $t = 2.63$, $p = .01$); (2) less elongation of the holes (Figure 11E; control aspect ratio $2.22 \pm .06$, $n = 24$; mutant 1.80 ± 0.03 , $n = 26$; $t = -6.73$, $p < .0001$); (3) poorer alignment to the centrifugal axis (Figure 11F; control angular deviation 7.13 ± 1.34 , $n = 24$; mutant 22.96 ± 3.47 , $n = 26$; $t = 4.23$, $p = .0002$); and (4) less angular coherence of hole polarity (Figure 11G; control angular coherence $0.65 \pm .03$, $n = 24$; mutant 0.36 ± 0.04 , $n = 26$; $t = -5.90$, $p < .0001$). Thus, in the absence of RGCs, astrocytes formed a network that lacked polarization along the centrifugal axis and was excessively variable in its density. This finding suggests that RGC–astrocyte interactions influence not only the initial migration of astrocyte somata but also the growth of their arbors during formation of the honeycomb-shaped vascular template.

4 | DISCUSSION

In this study, we report that astrocyte migration along RGC axons is an essential part of the mechanism determining astrocyte spatial pattern. In turn, astrocyte pattern is an essential contributor to vessel pattern, as we show in our astrocyte ablation experiments. Migrating astrocytes are intimately associated with RGC axons, and become polarized along them in a centrifugal orientation. In *Robo1/2*^{KO} mice, astrocytes assume aberrant orientations matching the abnormal trajectories of misguided axons, indicating that axons provide directional cues for astrocyte guidance. The functional importance of axon-derived cues was probed by studying astrocyte development in the absence of



RGCs using *Math5* mutant mice. We found that migrating astrocytes lose their orientation and fail to colonize peripheral retina in the absence of RGCs. Our results support a model in which retinal astrocytes migrate along RGC axons to colonize the retina and establish a template that stimulates and directs subsequent angiogenesis.

4.1 | Factors influencing migration of retinal astrocytes

As astrocytes migrate from the optic nerve head peripherally to cover the retina, their path through the RNFL lies in close apposition to the retinal inner limiting membrane (ILM), comprised of the endfeet of retinal progenitor cells and associated basement membrane. Astrocytes preferentially migrate on ILM substrate *in vitro*, and in mouse laminin mutants where the ILM becomes disrupted and patchy, astrocytes only enter RNFL regions overlying remaining ILM (Gnanaguru et al., 2013). Thus, the ILM provides a permissive substrate for astrocyte migration. However, factors that guide astrocytes from the optic nerve head to the retinal periphery remain unknown. In several species, including human, it has been noted that astrocytes move parallel to the direction of RGC axons (Chu et al., 2001; Fruttiger, 2007; Gariano & Gardner, 2005; Kubota & Suda, 2009; Provis et al., 1997). At one time it was thought, based on RGC axotomy studies in newborn cats, that axons were dispensable for astrocyte colonization of peripheral retina, but as GFAP was the astrocyte marker used for this study, it seems likely that GFAP⁺ immature astrocytes are already present in peripheral retina by birth in felines (Chan-Ling & Stone, 1991; Fruttiger, 2002). Thus, the question of how axons influence astrocyte migration has remained unresolved.

Here we demonstrate that immature astrocytes selectively colocalize with RGC axon fascicles (Figures 4 and 5), and that this association is functionally important for their dispersal across the retina (Figures 6 and 8) through orientating them in the centrifugal direction (Figures 5 and 7). Astrocytes did not depart the ILM even when given the option to do so by following misguided axons in *Robo1/2* mutants. Our results are therefore consistent with a model in which ILM attachment is essential for astrocyte migration, but directional information within the RNFL is provided by axons. Because axons themselves interact with the ILM, it is possible that mislocalization of axons or their secreted cues contribute to the astrocyte phenotypes in laminin mutants (Gnanaguru et al., 2013)

Our study provides a mechanistic explanation of previous observations that the astrocyte network is irregular and dysmorphic in mice lacking RGCs (Edwards et al., 2012). Because the number and distribution of astrocyte somata were not determined by Edwards et al., (2012), their observations were consistent with three possible RGC functions. First, RGCs have potent effects on astrocyte proliferation (Burne & Raff, 1997; Fruttiger et al., 1996), so their absence could disturb astrocyte pattern by influencing cell number. Second, the dysmorphic GFAP staining patterns might have resulted solely from altered astrocyte morphology, without any change in cell number. Finally, the altered network structure in *Math5* mutants might reflect defects in astrocyte migration. Here we investigated each of these possibilities.

We found that RGCs likely influence each of these developmental parameters. Total astrocyte numbers were transiently reduced in *Math5* mutants during the first postnatal week before recovering to control levels (Figure 8F). This phenotype can likely be ascribed at least in part to loss of RGC-derived mitogens. We also found some effects on astrocyte morphology that appear independent of cell number (Figure 11). However, our data support the notion that migration is the major mechanism through which astrocyte defects arise in the absence of RGCs. Together with our observations in wild-type and *Robo1/2*^{rkO} mice, this work supports the conclusion that axons provide guidance cues that direct migrating astrocytes out of central retina toward the periphery.

How do axons guide astrocytes? Owing to the precision with which astrocytes conform to axons, we favor the hypothesis that axons provide either a contact cue, or a secreted cue that acts at short range, perhaps by becoming affixed to the ILM basement membrane directly beneath axon fascicles. An intriguing candidate is PDGF-A, which is expressed by RGCs (Mudhar, Pollock, Wang, Stiles, & Richardson, 1993) and stimulates proliferation of retinal astrocytes (Fruttiger et al., 1996; Fruttiger, Calver, & Richardson, 2000) but has recently been shown to act as an astrocyte chemoattractant in *ex vivo* assays (Tao & Zhang, 2016). It was proposed that PDGF-A could be an RGC-derived guidance cue for centrifugal migration (Tao & Zhang, 2016), but as RGCs are at higher density in central than peripheral retina (Rodriguez et al., 2014; Wang et al., 2016), PDGF-A may not be well positioned to attract astrocytes to the periphery. By contrast, PDGF-A could act over short distances to attract astrocytes to axons. Our findings are consistent with a model in which PDGF-A ensures axonal contact, while axons themselves provide guidance cues for centrifugal migration. Further work will be required to test this model and to elucidate the molecular basis for axon-astrocyte interactions during migration.

4.2 | Fine-scale patterning of retinal astrocytes

Long-range migration is a prerequisite for normal astrocyte pattern formation, but other mechanisms clearly play a role. For example, astrocytes undergo short-range positional adjustments that arrange their somata into a mosaic, and they grow their arbors to form a network with characteristic honeycomb morphology. We show that interactions with RGCs contribute to both of these steps in astrocyte development (Figures 9 and 11). Additionally, other cell-cell interactions also likely contribute to these important patterning events. For example, as the honeycomb astrocyte morphology is morphologically distinct from the centripetally converging bundles of RGC axons, astrocytes must deviate from their RGC guides at some stage. Homotypic interactions between astrocytes may be important in this way (Chan-Ling & Stone, 1991; Distler et al., 1991). We see that astrocytes are always in contact with their neighbors, even at the wavefront of migration (Figures 1, 4, and 7), suggesting that they may coordinate their spacing and network morphology with each other. Furthermore, we found that astrocytes deprived of both RGC and vascular contact aggregate into large clumps (Figure 9), suggesting a propensity for homotypic aggregation that can be countered by interactions with their RNFL partners. The notion that

astrocyte morphology arises from an interplay between homotypic and RGC contacts is plausible based on our observations of individual astrocytes at the migration wavefront. These cells were sometimes seemed to contact more than one axon, thereby creating looping structures (Figure 2E). If early astrocytes can become a template for later-arriving ones through homotypic aggregation, these loops could provide the early substrate for honeycomb mesh formation.

4.3 | Patterning of retinal blood vessels

It has long been noted that astrocytes are well positioned to guide developmental angiogenesis, both because astrocytes develop first and because of the striking colocalization of vessels with astrocytes (Gariano, Sage, Kaplan, & Hendrickson, 1996; Jiang, Bezhadian, & Caldwell, 1995; Stone & Dreher, 1987; Stone et al., 1995). Several past experiments are consistent with the notion that astrocytes are necessary for vessel patterning, but lack the strict cell-type specificity required to serve as a critical test of the template hypothesis. First, Fruttiger et al. (1996) showed that overexpression of PDGF-A, a ligand for the astrocyte receptor PDGFR α , causes overelaboration of astrocyte and vascular networks, while sequestration of PDGF using soluble PDGFR α decoy receptor caused underelaboration of both networks. However, PDGFR α can also sequester PDGF-B, a ligand for the endothelial cell receptor PDGFR β (Betsholtz, 1995; Mudhar et al., 1993). Moreover, PDGF-A can dimerize with PDGF-B to mediate signaling through PDGFR β in some cases (Betsholtz, 1995). Thus, these manipulations might have directly affected both cell types. Second, in laminin mutants where ILM formation and astrocyte colonization are patchy, blood vessels only form in astrocyte-containing regions (Gnanaguru et al., 2013). However, these astrocyte-containing regions are also the only ILM-containing regions, so the guidance cue responsible for vessel development might be derived from the ILM itself rather than from astrocytes. Finally, mice lacking the Tlx transcription factor have been cited in favor of the template hypothesis. These animals have a phenotype resembling in some ways the *Math5* mutants: an aberrant astrocyte network forms, but intrinsic retinal vasculature is completely absent, and hyaloid vessels fail to regress (Edwards et al., 2012; Uemura et al., 2006; Figure 6). In both mutants, absence of intrinsic vessels might be due to the aberrant astrocytes, but other causes are also plausible. Tlx is also expressed in retinal progenitor cells, so the cell type originating the vascular phenotype is unclear. And because axons help to pattern the nascent optic nerve and the optic nerve head (Brown et al., 2001), it is possible that endothelial cells cannot access the neural retina in *Math5* mutants.

Two recent studies demonstrate that different specific manipulations of astrocytes, conditional knockout of HIF-2 α (Duan et al., 2014) or PDGFR α (Tao & Zhang, 2016), disrupt vascular development. These reports provide the first direct experimental evidence that astrocytes can modulate developmental angiogenesis in a manner reminiscent of their role in pathological neovascularization (Dorrell et al., 2010; Weidemann et al., 2010). However, because the ablation of vessels (and astrocytes in the PDGFR α case) is so complete in these mutants, it is impossible to assess whether the mechanism of vessel loss includes a

requirement that angiogenesis follow an astrocyte template. Furthermore, these studies leave open the possibility that the knockout astrocytes might have pathological gain-of-function phenotypes that prevent angiogenesis.

For these reasons, we used a different approach to directly test the idea that astrocytes are required for blood vessel development. We show that the *GFAP-Cre* mouse line we used (Zhuo et al., 2001) is highly astrocyte-specific during early postnatal development, and that it can drive selective elimination of astrocytes using the DTR-DT system. Systemic DT administration at P0 reduced astrocyte number with variable efficiency, possibly due to variability in Cre expression in our *GFAP-Cre* line at early postnatal ages, efficacy of the DT dose, and/or mortality associated with high efficiency deletion of GFAP⁺ cells elsewhere in the body. Intraocular DT administration was required at P5 to avoid lethality, supporting the idea that overall Cre expression levels were lower at P0. The variability of P0 ablation efficiency did, however, have an advantage, in that it allowed us to observe that vascular effects were only seen in eyes with successful astrocyte depletion. When astrocytes were ablated prior to onset of angiogenesis, vascular complexity was decreased in proportion to the reduction in astrocyte density, but the few vessels present still conformed to the network of remaining astrocytes. When astrocytes were ablated during angiogenesis, advance of the vascular wavefront was inhibited, with wavefront vessels assuming inappropriate morphologies. The implications of these results are twofold: (1) astrocytes quantitatively stimulate vessel growth and (2) astrocytes qualitatively determine the pattern of vessel growth. Our study thus provides compelling evidence that astrocytes guide vascular development, thereby providing important support for a major hypothesis in this field.

How might astrocytes promote angiogenesis? As astrocytes can both stimulate vessel growth and determine vessel growth patterns, astrocytes appear to provide two kinds of signals: (1) angiogenic growth factors and (2) contact-mediated cues for endothelial cell guidance. An obvious candidate in the first category is vascular endothelial growth factor (VEGF), which is expressed by astrocytes in avascular regions of the developing retina (Kubota, Hirashima, Kishi, Stewart, & Suda, 2008; Stone et al., 1995; West, Richardson, & Fruttiger, 2005) and is involved in retinal angiogenesis (Gerhardt et al., 2003; Stalmans et al., 2002; Uemura et al., 2006). However, astrocytic VEGF is not required for normal vascular development, suggesting that another VEGF source can be used when astrocytic VEGF disappears (Scott et al., 2010). Thus, the effects of astrocyte ablation are unlikely to be explained solely by VEGF removal. It will be important to examine the role of additional growth factors in this system. As for contact-mediated guidance cues, many ECM components and interactors such as laminins (Gnanaguru et al., 2013), integrins (Hirota et al., 2011; Samarelli et al., 2014), dystrophin (Giocanti-Auregan et al., 2016), and proteoglycans (Stenzel et al., 2011) are very likely involved. However, their widespread expression makes these unlikely candidates to mediate a specific astrocyte–endothelial interaction. R-cadherin may act as an adhesion molecule for astrocyte–vessel interactions, but functional data on its precise role remain unclear (Dorrell, Aguilar, & Friedlander,



2002; Fruttiger, 2007). At this juncture, it remains unknown whether a specific astrocyte–endothelial protein–protein interaction exists to pattern angiogenesis, or if a set of general and partially redundant mechanisms is involved. Further work will be required to gain molecular insight into this process.

Our ablation studies also suggest that astrocytes play a role in maintaining vessels that have already colonized the RNFL. While a thorough analysis of this phenotype is beyond the scope of this study, the continuing interactions between astrocytes and vasculature at later stages of development certainly merit further inquiry. It is clear that the colonization stage of vascular development we address here is only the first of many developmental mechanisms that determine the ultimate form of the vascular network. In addition to neuro–glial–vascular interactions, these later mechanisms are also likely to include contributions from microglia and pericytes (Benjamin, Hemo, & Keshet, 1998; Chan-Ling, 1994; Tata, Ruhrberg, & Fantin, 2015).

4.4 | Implications for pathogenesis of ROP

In ROP, the anterior extension of retinal vasculature is halted in the mid-periphery, leaving the peripheral retina ischemic. The resulting hypoxia triggers a second, neovascular phase of ROP pathogenesis, producing pathological vessels prone to bleeding that cause the most serious complications of ROP. This neovascular phase of ROP has been extensively studied, and effective therapeutic strategies exist to mitigate damage by neovascularization, but understanding why some cases of ROP are self-limited and others have persistent vascular abnormalities is poorly understood (Hellstrom et al., 2013). Hyperoxia, the major known modifiable risk factor for ROP, likely exerts direct effects on blood vessels, but given that vessels appear to follow an astrocyte template it is possible that astrocyte patterning is also affected by hyperoxia (Chan-Ling & Stone, 1992). Astrocyte aggregates have been found in human ROP histopathological specimens at the transition zone between vascular and avascular retina (Sun, Dalal, & Gariano, 2010), suggesting that the centrifugal migration of astrocytes, like that of blood vessels, may be arrested. We speculate that the cellular processes we describe here—RGC-guided astrocyte migration and astrocyte-directed angiogenesis—may be affected in ROP.

5 | CONCLUSIONS

Here we have established that a series of interactions between RGCs, astrocytes, and blood vessels play important roles in retinal development. Insight into these cellular mechanisms will likely have bearing on the pathobiology of ROP and the basic mechanisms by which retinal tissue becomes vascularized. Moreover, they might have broader significance for brain vascularization. In the cerebral cortex, large penetrating vessels exist before astrocytes, but astrocyte differentiation appears to coincide with elaboration of dense capillaries (Gerhardt et al., 2004; Ma et al., 2012; Ogunshola et al., 2000; Robertson, Du Bois, Bowman, & Goldstein, 1985). This observation raises the possibility that signals transmitted between astrocytes, neurons, and endothelial cells are conserved between retina and brain. In this

case, the retina will serve as a useful model to uncover these fundamental mechanisms.

ACKNOWLEDGMENT

Financial support was provided by the National Eye Institute (R01EY024694 to JNK.; Core grant EY5722 to Duke University); Ruth K. Broad Foundation (MLO'S); National Science Foundation (Graduate Research Fellowship DGE-1644868 to VMP); Pew Charitable Trusts, E. Matilda Ziegler Foundation, McKnight Endowment Fund for Neuroscience, Alfred P. Sloan foundation, and a Holland-Trice Scholars Award (JNK); and Research to Prevent Blindness Unrestricted Grant (Duke University). Thanks to Nicholas Brecha (UCLA) for sharing the RBPMS antibody, Daniel Saban (Duke University) for cDTR mice, Brigid Hogan (Duke University) for fGFP mice, Joshua Weiner (University of Iowa) for Pax2-Cre mice, Le Ma (Thomas Jefferson University) and Weinang Lu (Boston University) for Robo1 and Robo2 mutant mice, and Ariane Pereira and Megan Stogsdill for mouse colony management. The authors declare no competing financial interests.

REFERENCES

- Benjamin, L. E., Hemo, I., & Keshet, E. (1998). A plasticity window for blood vessel remodelling is defined by pericyte coverage of the preformed endothelial network and is regulated by PDGF-B and VEGF. *Development*, *125*, 1591–1598.
- Betsholtz, C. (1995). Role of platelet-derived growth factors in mouse development. *International Journal of Developmental Biology*, *39*, 817–825.
- Brown, N. L., Kanekar, S., Vetter, M. L., Tucker, P. K., Gemza, D. L., & Glaser, T. (1998). Math5 encodes a murine basic helix-loop-helix transcription factor expressed during early stages of retinal neurogenesis. *Development*, *125*, 4821–4833.
- Brown, N. L., Patel, S., Brzezinski, J., & Glaser, T. (2001). Math5 is required for retinal ganglion cell and optic nerve formation. *Development*, *128*, 2497–2508.
- Buch, T., Heppner, F. L., Tertilt, C., Heinen, T. J., Kremer, M., Wunderlich, F. T., . . . , Waisman, A. (2005). A Cre-inducible diphtheria toxin receptor mediates cell lineage ablation after toxin administration. *Nature Methods*, *2*, 419–426.
- Burne, J. F., & Raff, M. C. (1997). Retinal ganglion cell axons drive the proliferation of astrocytes in the developing rodent optic nerve. *Neuron*, *18*, 223–230.
- Burne, J. F., Staple, J. K., & Raff, M. C. (1996). Glial cells are increased proportionally in transgenic optic nerves with increased numbers of axons. *Journal of Neuroscience*, *16*, 2064–2073.
- Chan-Ling, T. (1994). Glial, neuronal and vascular interactions in the mammalian retina. *Progress in Retinal and Eye Research*, *13*, 357–389.
- Chan-Ling, T., Chu, Y., Baxter, L., Weible li, M., & Hughes, S. (2009). In vivo characterization of astrocyte precursor cells (APCs) and astrocytes in developing rat retinae: Differentiation, proliferation, and apoptosis. *Glia*, *57*, 39–53.
- Chan-Ling, T., McLeod, D. S., Hughes, S., Baxter, L., Chu, Y., Hasegawa, T., & Luty, G. A. (2004). Astrocyte-endothelial cell relationships during human retinal vascular development. *Investigative Ophthalmology & Visual Science*, *45*, 2020–2032.

- Chan-Ling, T., & Stone, J. (1991). Factors determining the migration of astrocytes into the developing retina: Migration does not depend on intact axons or patent vessels. *Journal of Comparative Neurology*, *303*, 375–386.
- Chan-Ling, T., & Stone, J. (1992). Degeneration of astrocytes in feline retinopathy of prematurity causes failure of the blood-retinal barrier. *Investigative Ophthalmology & Visual Science*, *33*, 2148–2159.
- Chu, Y., Hughes, S., & Chan-Ling, T. (2001). Differentiation and migration of astrocyte precursor cells and astrocytes in human fetal retina: Relevance to optic nerve coloboma. *FASEB Journal*, *15*, 2013–2015.
- Colello, R. J., & Guillery, R. W. (1990). The early development of retinal ganglion cells with uncrossed axons in the mouse: Retinal position and axonal course. *Development*, *108*, 515–523.
- Dakubo, G. D., Beug, S. T., Mazerolle, C. J., Thurig, S., Wang, Y., & Wallace, V. A. (2008). Control of glial precursor cell development in the mouse optic nerve by sonic hedgehog from retinal ganglion cells. *Brain Research*, *1228*, 27–42.
- Dakubo, G. D., Wang, Y. P., Mazerolle, C., Campsall, K., McMahon, A. P., & Wallace, V. A. (2003). Retinal ganglion cell-derived sonic hedgehog signaling is required for optic disc and stalk neuroepithelial cell development. *Development*, *130*, 2967–2980.
- Distler, C., Dreher, Z., & Stone, J. (1991). Contact spacing among astrocytes in the central nervous system: An hypothesis of their structural role. *Glia*, *4*, 484–494.
- Domyan, E. T., Branchfield, K., Gibson, D. A., Naiche, L. A., Lewandoski, M., Tessier-Lavigne, M., . . . , Sun, X. (2013). Roundabout receptors are critical for foregut separation from the body wall. *Developmental Cell*, *24*, 52–63.
- Dorrell, M. I., Aguilar, E., & Friedlander, M. (2002). Retinal vascular development is mediated by endothelial filopodia, a preexisting astrocytic template and specific R-cadherin adhesion. *Investigative Ophthalmology & Visual Science*, *43*, 3500–3510.
- Dorrell, M. I., Aguilar, E., Jacobson, R., Trauger, S. A., Friedlander, J., Siuzdak, G., & Friedlander, M. (2010). Maintaining retinal astrocytes normalizes revascularization and prevents vascular pathology associated with oxygen-induced retinopathy. *Glia*, *58*, 43–54.
- Duan, L. J., Takeda, K., & Fong, G. H. (2014). Hypoxia inducible factor-2alpha regulates the development of retinal astrocytic network by maintaining adequate supply of astrocyte progenitors. *PLoS One*, *9*, e84736.
- Edwards, M. M., McLeod, D. S., Li, R., Grebe, R., Bhutto, I., Mu, X., & Lutty, G. A. (2012). The deletion of Math5 disrupts retinal blood vessel and glial development in mice. *Experimental Eye Research*, *96*, 147–156.
- Fruttiger, M. (2002). Development of the mouse retinal vasculature: Angiogenesis versus vasculogenesis. *Investigative Ophthalmology & Visual Science*, *43*, 522–527.
- Fruttiger, M. (2007). Development of the retinal vasculature. *Angiogenesis*, *10*, 77–88.
- Fruttiger, M., Calver, A. R., Kruger, W. H., Mudhar, H. S., Michalovich, D., Takakura, N., . . . , Richardson, W. D. (1996). PDGF mediates a neuron-astrocyte interaction in the developing retina. *Neuron*, *17*, 1117–1131.
- Fruttiger, M., Calver, A. R., & Richardson, W. D. (2000). Platelet-derived growth factor is constitutively secreted from neuronal cell bodies but not from axons. *Current Biology*, *10*, 1283–1286.
- Furuta, Y., Lagutin, O., Hogan, B. L., & Oliver, G. C. (2000). Retina- and ventral forebrain-specific Cre recombinase activity in transgenic mice. *Genesis*, *26*, 130.
- Gariano, R. F., & Gardner, T. W. (2005). Retinal angiogenesis in development and disease. *Nature*, *438*, 960–966.
- Gariano, R. F., Sage, E. H., Kaplan, H. J., & Hendrickson, A. E. (1996). Development of astrocytes and their relation to blood vessels in fetal monkey retina. *Investigative Ophthalmology & Visual Science*, *37*, 2367–2375.
- Gerhardt, H., Golding, M., Fruttiger, M., Ruhrberg, C., Lundkvist, A., Abramsson, A., . . . , Shima, D. (2003). VEGF guides angiogenic sprouting utilizing endothelial tip cell filopodia. *Journal of Cell Biology*, *161*, 1163–1177.
- Gerhardt, H., Ruhrberg, C., Abramsson, A., Fujisawa, H., Shima, D., & Betsholtz, C. (2004). Neuropilin-1 is required for endothelial tip cell guidance in the developing central nervous system. *Developmental Dynamics*, *231*, 503–509.
- Giocanti-Auregan, A., Vacca, O., Benard, R., Cao, S., Siqueiros, L., Montanez, C., . . . , Guillonnet, X. (2016). Altered astrocyte morphology and vascular development in dystrophin-Dp71-null mice. *Glia*, *64*, 716–729.
- Gnanaguru, G., Bachay, G., Biswas, S., Pinzon-Duarte, G., Hunter, D. D., & Brunken, W. J. (2013). Laminins containing the beta2 and gamma3 chains regulate astrocyte migration and angiogenesis in the retina. *Development*, *140*, 2050–2060.
- Hellstrom, A., Smith, L. E., & Dammann, O. (2013). Retinopathy of prematurity. *Lancet*, *382*, 1445–1457.
- Hirota, S., Liu, Q., Lee, H. S., Hossain, M. G., Lacy-Hulbert, A., & McCarty, J. H. (2011). The astrocyte-expressed integrin alpha5beta1 governs blood vessel sprouting in the developing retina. *Development*, *138*, 5157–5166.
- Huxlin, K. R., Sefton, A. J., & Furby, J. H. (1992). The origin and development of retinal astrocytes in the mouse. *Journal of Neurocytology*, *21*, 530–544.
- Jiang, B., Bezhadian, M. A., & Caldwell, R. B. (1995). Astrocytes modulate retinal vasculogenesis: Effects on endothelial cell differentiation. *Glia*, *15*, 1–10.
- Kay, J. N., Chu, M. W., & Sanes, J. R. (2012). MEGF10 and MEGF11 mediate homotypic interactions required for mosaic spacing of retinal neurons. *Nature*, *483*, 465–469.
- Kubota, Y., Hirashima, M., Kishi, K., Stewart, C. L., & Suda, T. (2008). Leukemia inhibitory factor regulates microvessel density by modulating oxygen-dependent VEGF expression in mice. *Journal of Clinical Investigation*, *118*, 2393–2403.
- Kubota, Y., & Suda, T. (2009). Feedback mechanism between blood vessels and astrocytes in retinal vascular development. *Trends in Cardiovascular Medicine*, *19*, 38–43.
- Long, H., Sabatier, C., Ma, L., Plump, A., Yuan, W., Ornitz, D. M., . . . , Tessier-Lavigne, M. (2004). Conserved roles for Slit and Robo proteins in midline commissural axon guidance. *Neuron*, *42*, 213–223.
- Lu, W., van Eerde, A. M., Fan, X., Quintero-Rivera, F., Kulkarni, S., Ferguson, H., . . . , Li, Q. G. (2007). Disruption of ROBO2 is associated with urinary tract anomalies and confers risk of vesicoureteral reflux. *American Journal of Human Genetics*, *80*, 616–632.
- Ma, S., Kwon, H. J., & Huang, Z. (2012). A functional requirement for astroglia in promoting blood vessel development in the early postnatal brain. *PLoS One*, *7*, e48001.
- Madisen, L., Zwingman, T. A., Sunkin, S. M., Oh, S. W., Zariwala, H. A., Gu, H., . . . , Jones, A. R. (2010). A robust and high-throughput Cre reporting and characterization system for the whole mouse brain. *Nature Neuroscience*, *13*, 133–140.
- Mudhar, H. S., Pollock, R. A., Wang, C., Stiles, C. D., & Richardson, W. D. (1993). PDGF and its receptors in the developing rodent retina and optic nerve. *Development*, *118*, 539–552.
- Muzumdar, M. D., Tasic, B., Miyamichi, K., Li, L., & Luo, L. (2007). A global double-fluorescent Cre reporter mouse. *Genesis*, *45*, 593–605.



- Ogunshola, O. O., Stewart, W. B., Mihalcik, V., Solli, T., Madri, J. A., & Ment, L. R. (2000). Neuronal VEGF expression correlates with angiogenesis in postnatal developing rat brain. *Developmental Brain Research*, *119*, 139–153.
- Ohyama, T., & Groves, A. K. (2004). Generation of Pax2-Cre mice by modification of a Pax2 bacterial artificial chromosome. *Genesis*, *38*, 195–199.
- Provis, J. M., Leech, J., Diaz, C. M., Penfold, P. L., Stone, J., & Keshet, E. (1997). Development of the human retinal vasculature: Cellular relations and VEGF expression. *Experimental Eye Research*, *65*, 555–568.
- Rama, N., Dubrac, A., Mathivet, T., Ni Charthaigh, R. A., Genet, G., Cristofaro, B., . . . , Chedotal, A. (2015). Slit2 signaling through Robo1 and Robo2 is required for retinal neovascularization. *Nature Medicine*, *21*, 483–491.
- Raven, M. A., Eglen, S. J., Ohab, J. J., & Reese, B. E. (2003). Determinants of the exclusion zone in dopaminergic amacrine cell mosaics. *Journal of Comparative Neurology*, *461*, 123–136.
- Rawlins, E. L., Okubo, T., Xue, Y., Brass, D. M., Auten, R. L., Hasegawa, H., . . . , Hogan, B. L. (2009). The role of Scgb1a1+ Clara cells in the long-term maintenance and repair of lung airway, but not alveolar, epithelium. *Cell Stem Cell*, *4*, 525–534.
- Robertson, P. L., Du Bois, M., Bowman, P. D., & Goldstein, G. W. (1985). Angiogenesis in developing rat brain: An in vivo and in vitro study. *Brain Research*, *355*, 219–223.
- Rodieck, R. W. (1991). The density recovery profile: A method for the analysis of points in the plane applicable to retinal studies. *Visual Neuroscience*, *6*, 95–111.
- Rodriguez, A. R., de Sevilla Muller, L. P., & Brecha, N. C. (2014). The RNA binding protein RBPMS is a selective marker of ganglion cells in the mammalian retina. *Journal of Comparative Neurology*, *522*, 1411–1443.
- Samarelli, A. V., Riccitelli, E., Bizzozero, L., Silveira, T. N., Seano, G., Pergolizzi, M., . . . , Bottos, A. (2014). Neuroligin 1 induces blood vessel maturation by cooperating with the alpha6 integrin. *Journal of Biological Chemistry*, *289*, 19466–19476.
- Scott, A., Powner, M. B., Gandhi, P., Clarkin, C., Gutmann, D. H., Johnson, R. S., . . . , Fruttiger, M. (2010). Astrocyte-derived vascular endothelial growth factor stabilizes vessels in the developing retinal vasculature. *PLoS One*, *5*, e11863.
- Stalmans, I., Ng, Y. S., Rohan, R., Fruttiger, M., Bouche, A., Yuce, A., . . . , Jansen, S. (2002). Arteriolar and venular patterning in retinas of mice selectively expressing VEGF isoforms. *Journal of Clinical Investigation*, *109*, 327–336.
- Stenzel, D., Lundkvist, A., Sauvaget, D., Busse, M., Graupera, M., van der Flier, A., . . . , Costell, M. (2011). Integrin-dependent and -independent functions of astrocytic fibronectin in retinal angiogenesis. *Development*, *138*, 4451–4463.
- Stone, J., & Dreher, Z. (1987). Relationship between astrocytes, ganglion cells and vasculature of the retina. *Journal of Comparative Neurology*, *255*, 35–49.
- Stone, J., Itin, A., Alon, T., Pe'er, J., Gnessin, H., Chan-Ling, T., & Keshet, E. (1995). Development of retinal vasculature is mediated by hypoxia-induced vascular endothelial growth factor (VEGF) expression by neuroglia. *Journal of Neuroscience*, *15*, 4738–4747.
- Sun, Y., Dalal, R., & Gariano, R. F. (2010). Cellular composition of the ridge in retinopathy of prematurity. *Archives of Ophthalmology*, *128*, 638–641.
- Tao, C., & Zhang, X. (2014). Development of astrocytes in the vertebrate eye. *Developmental Dynamics*, *243*, 1501–1510.
- Tao, C., & Zhang, X. (2016). Retinal proteoglycans act as cellular receptors for basement membrane assembly to control astrocyte migration and angiogenesis. *Cell Reports*, *17*, 1832–1844.
- Tata, M., Ruhrberg, C., & Fantin, A. (2015). Vascularisation of the central nervous system. *Mechanisms of Development*, *138 Pt 1*, 26–36.
- Thompson, H., Andrews, W., Parnavelas, J. G., & Erskine, L. (2009). Robo2 is required for Slit-mediated intraretinal axon guidance. *Developmental Biology*, *335*, 418–426.
- Thompson, H., Camand, O., Barker, D., & Erskine, L. (2006). Slit proteins regulate distinct aspects of retinal ganglion cell axon guidance within dorsal and ventral retina. *Journal of Neuroscience*, *26*, 8082–8091.
- Tout, S., Dreher, Z., Chan-Ling, T., & Stone, J. (1993). Contact-spacing among astrocytes is independent of neighbouring structures: In vivo and in vitro evidence. *Journal of Comparative Neurology*, *332*, 433–443.
- Uemura, A., Kusuhara, S., Wiegand, S. J., Yu, R. T., & Nishikawa, S. (2006). Tlx acts as a proangiogenic switch by regulating extracellular assembly of fibronectin matrices in retinal astrocytes. *Journal of Clinical Investigation*, *116*, 369–377.
- Wallace, V. A., & Raff, M. C. (1999). A role for Sonic hedgehog in axon-to-astrocyte signalling in the rodent optic nerve. *Development*, *126*, 2901–2909.
- Wang, J., O'Sullivan, M. L., Mukherjee, D., Punal, V. M., Farsiu, S., & Kay, J. N. (2016). Anatomy and spatial organization of Muller glia in mouse retina. *Journal of Comparative Neurology*.
- Wang, S. W., Kim, B. S., Ding, K., Wang, H., Sun, D., Johnson, R. L., . . . , Gan, L. (2001). Requirement for math5 in the development of retinal ganglion cells. *Genes & Development*, *15*, 24–29.
- Watanabe, T., & Raff, M. C. (1988). Retinal astrocytes are immigrants from the optic nerve. *Nature*, *332*, 834–837.
- Weidemann, A., Krohne, T. U., Aguilar, E., Kurihara, T., Takeda, N., Dorell, M. I., . . . , Johnson, R. S. (2010). Astrocyte hypoxic response is essential for pathological but not developmental angiogenesis of the retina. *Glia*, *58*, 1177–1185.
- West, H., Richardson, W. D., & Fruttiger, M. (2005). Stabilization of the retinal vascular network by reciprocal feedback between blood vessels and astrocytes. *Development*, *132*, 1855–1862.
- Zhuo, L., Theis, M., Alvarez-Maya, I., Brenner, M., Willecke, K., & Messing, A. (2001). hGFAP-cre transgenic mice for manipulation of glial and neuronal function in vivo. *Genesis*, *31*, 85–94.

How to cite this article: O'Sullivan ML, Puñal VM, Kerstein PC, et al. Astrocytes follow ganglion cell axons to establish an angiogenic template during retinal development. *Glia*. 2017;65:1697–1716. <https://doi.org/10.1002/glia.23189>